

Variation of Absorption Ångström Exponent in Aerosols From Different Emission Sources

Key Points:

- Absorption Ångström exponent (AAE) values were on average the highest in shipping and small-scale wood combustion emissions
- AAE values were the lowest in aerosols originating from ethanol-fueled bus and coal-fired power plant emissions
- The results raise the awareness of the possible shortcoming in using AAE for aerosol characterization particularly in fresh emissions

Supporting Information:

Supporting Information may be found in the online version of this article.

Correspondence to:

















A. Helin,
aku.helin@fmi.fi

Citation:

Helin, A., Virkkula, A., Backman, J., Pirjola, L., Sippula, O., Aakko-Saksa, P., et al. (2021). Variation of absorption Ångström exponent in aerosols from different emission sources. *Journal of Geophysical Research: Atmospheres*, 126, e2020JD034094. <https://doi.org/10.1029/2020JD034094>

Received 15 OCT 2020

Accepted 10 APR 2021

A. Helin¹ , A. Virkkula¹ , J. Backman¹ , L. Pirjola^{2,3} , O. Sippula^{4,5} , P. Aakko-Saksa⁶ , S. Väätäinen⁴, F. Mylläri⁷ , A. Järvinen⁷ , M. Bloss¹, M. Aurela¹ , G. Jakobi^{8,9} , P. Karjalainen⁷ , R. Zimmermann^{8,9,10} , J. Jokiniemi⁴ , S. Saarikoski¹ , J. Tissari⁴ , T. Rönkkö⁷ , J. V. Niemi¹¹ , and H. Timonen¹ 

¹Atmospheric Composition Research, Finnish Meteorological Institute, Helsinki, Finland, ²Department of Technology, Metropolia University of Applied Sciences, Helsinki, Finland, ³Department of Physics, University of Helsinki, Helsinki, Finland, ⁴Department of Environmental and Biological Sciences, University of Eastern Finland, Kuopio, Finland, ⁵Department of Chemistry, University of Eastern Finland, Joensuu, Finland, ⁶VTT Technical Research Centre of Finland, Finland, ⁷Aerosol Physics Laboratory, Physics Unit, Tampere University, Tampere University, Finland, ⁸Joint Mass Spectrometry Centre, Cooperation Group Comprehensive Molecular Analytics, Helmholtz Zentrum München, Neuherberg, Germany, ⁹Helmholtz Virtual Institute for Complex Molecular Systems in Environmental Health, Neuherberg, Germany, ¹⁰Analytical Chemistry, Institute of Chemistry, University of Rostock, Rostock, Germany, ¹¹Helsinki Region Environmental Services Authority, Helsinki, Finland

Abstract The absorption Ångström exponent (AAE) describes the spectral dependence of light absorption by aerosols. AAE is typically used to differentiate between different aerosol types for example., black carbon, brown carbon, and dust particles. In this study, the variation of AAE was investigated mainly in fresh aerosol emissions from different fuel and combustion types, including emissions from ships, buses, coal-fired power plants, and residential wood burning. The results were assembled to provide a compendium of AAE values from different emission sources. A dual-spot aethalometer (AE33) was used in all measurements to obtain the light absorption coefficients at seven wavelengths (370–950 nm). AAE_{470/950} varied greatly between the different emission sources, ranging from -0.2 ± 0.7 to 3.0 ± 0.8 . The correlation between the AAE_{470/950} and AAE₃₇₀₋₉₅₀ results was good ($R^2 = 0.95$) and the mean bias error between these was 0.02. In the ship engine exhaust emissions, the highest AAE_{470/950} values (up to 2.0 ± 0.1) were observed when high sulfur content heavy fuel oil was used, whereas low sulfur content fuels had the lowest AAE_{470/950} ($0.9-1.1$). In the diesel bus exhaust emissions, AAE_{470/950} increased in the order of acceleration (0.8 ± 0.1), deceleration (1.1 ± 0.1), and steady driving (1.2 ± 0.1). In the coal-fired power plant emissions, the variation of AAE_{470/950} was substantial (from -0.1 ± 2.1 to 0.9 ± 1.6) due to the differences in the fuels and flue gas cleaning conditions. Fresh wood-burning derived aerosols had AAE_{470/950} from 1.1 ± 0.1 (modern masonry heater) to 1.4 ± 0.1 (pellet boiler), lower than typically associated with wood burning, while the burn cycle phase affected AAE variation.

1. Introduction

The absorption Ångström exponent (AAE) describes the spectral dependence of light absorption by aerosols. AAE can be used for aerosol characterization (Bond et al., 2013), and it can be applied for the source apportionment of black carbon (BC) and carbonaceous matter (CM) (Forello et al., 2019; Herich et al., 2011; Sandradewi, Prévôt, Szidat, et al., 2008; Zotter et al., 2017). The wavelength (λ) dependence of the light absorption coefficient ($b_{\text{abs}}[\lambda]$) can be approximated to follow a power-law relationship: $b_{\text{abs}}(\lambda) \propto \lambda^{-\text{AAE}}$ (Kirchstetter & Thatcher, 2012; Moosmüller et al., 2009). For pure BC particles, the AAE is approximately 1, indicating “weak” spectral dependence of light absorption (Andreae & Gelencsér, 2006; Bond & Bergstrom, 2006; Bond et al., 2013; Moosmüller et al., 2009). When the AAE >> 1, it is often considered to be an indication of the presence of other light-absorbing components, such as organic aerosols and/or mineral dust (Andreae & Gelencsér, 2006; Laskin et al., 2015; Moosmüller et al., 2009). The light-absorbing part of organic aerosols is commonly referred to as brown carbon (BrC); a heterogeneous group of compounds from both primary and secondary sources (Andreae & Gelencsér, 2006; Kirchstetter et al., 2004; Laskin et al., 2015). Both BrC and mineral dust particles absorb light relatively stronger at the near-ultraviolet (UV) wavelengths than at the near-infrared (IR) wavelengths (Bond et al., 2013; Moosmüller et al., 2009),

© 2021. The Authors.

This is an open access article under the terms of the [Creative Commons Attribution License](https://creativecommons.org/licenses/by/4.0/), which permits use, distribution and reproduction in any medium, provided the original work is properly cited.

resulting in high AAE values, e.g., ranging from ~ 2 to ~ 10 (Caponi et al., 2017; Laskin et al., 2015; Pokhrel et al., 2016). Consequently, AAE can be used as a proxy to characterize the aerosol composition, namely to indicate the presence BC, BrC, and dust. AAE has gained ground in becoming one of the most used optical parameters solely applied to discriminate between these types of aerosol species (Goetz et al., 2018; Olson et al., 2015).

Since the early 2000s it has been a common standard in the literature, in studies addressing aerosol optical characteristics, to use approximately $AAE = 1$ as an indication of BC and $AAE > 1$ as an indication of BrC. In general, these simplified AAE threshold values are supported to some extent by both experimental (laboratory and ambient measurements) and theoretical modeling studies (Kirchstetter et al., 2004; Lack & Langridge, 2013; Moosmüller et al., 2009). However, multiple different factors affect the AAE. Even for pure BC particles, the AAE can vary depending on, for example, particle morphology and size (Gyawali et al., 2009; Li et al., 2016; Liu et al., 2018; Liu et al., 2015). In principle, following simple Mie theory core-shell modeling, the threshold $AAE = 1$ for BC is valid for externally mixed pure BC particles with core diameters of approximately < 100 nm (Gyawali et al., 2009; Lack & Cappa, 2010; Virkkula, 2020). The situation becomes more complicated when, for example, the BC particles are larger, coated with either non-absorbing or absorbing coating, and the relative core/shell coating thickness varies (Gyawali et al., 2009; Lack & Cappa, 2010; Virkkula, 2020; Wu et al., 2018). Under these conditions, the AAE values may range for example, from -0.2 to 1.7 for BC internally mixed with organic carbon (Gyawali et al., 2009; Virkkula, 2020). Furthermore, if the pure BC particles are significantly larger than ~ 200 – 300 nm, the AAE may approach negative values (Gyawali et al., 2009; Lack & Cappa, 2010; Virkkula, 2020). In addition, the method and wavelength ranges used for AAE calculation affect the output AAE values (discussed later on). Consequently, differentiation of BC, BrC, and dust solely based on AAE may not be quantitatively accurate. Auxiliary measurements to support the aerosol characterization would require information about the BC particle size, coating thickness, chemical composition of coating and particle morphology, etc. In practice, this is not feasible for a single instrument and some assumptions need to be made beforehand. These uncertainties, however, do not undermine the importance of knowing the AAE of different aerosol types as derived from filter-based instruments such as the one used in this study.

As mentioned at the beginning, AAE can be also used for the source apportionment of BC and CM. Nowadays, perhaps the most commonly applied source apportionment method is known as the Aethalometer model (Briggs & Long, 2016; Herich et al., 2011; Sandradewi, Prévôt, Weingartner, et al., 2008; Sandradewi, Prévôt, Szidat, et al., 2008). This source apportionment model has been central in a number of studies in recent years (Becerril-Valle et al., 2017; Crilley et al., 2015; Diapouli et al., 2017; Jereb et al., 2018; Martinsson et al., 2017; Rajesh & Ramachandran, 2017; Resquin et al., 2018; Titos et al., 2017; Zhu et al., 2017). Briefly, the Aethalometer model quantifies BC/CM from fossil fuel and biomass burning sources based on the spectral dependence of light absorption [Herich et al., 2011; Sandradewi, Prévôt, Szidat, et al., 2008; Zotter et al., 2017]. In the Aethalometer model, it is assumed that the measured total light absorption is solely due to aerosols derived from fossil fuel and biomass burning sources (Sandradewi, Prévôt, Szidat, et al., 2008).

The Aethalometer model utilizes user-selected a priori AAE values to apportion BC/CM from the two sources by implementing specified AAE values for both sources. For example, typically AAE for BC from fossil fuel sources (AAE_{FF}) is fixed to ~ 1 , and AAE for BC from biomass burning sources (AAE_{BB}) is fixed to ~ 2 . Even though the Aethalometer model is somewhat simplified and not necessarily adequate for all places and seasons (Garg et al., 2015; Harrison et al., 2012, 2013), it has been widely accepted and used to quantify BC/CM sources at different sites. The main concern and source of uncertainty related to the usage of the Aethalometer model is the selection of the fixed AAE_{FF} and AAE_{BB} values to which the model is highly sensitive. For some sampling sites and environments, the selection of suitable AAE values may be challenging if the BC and/or CM emission sources are substantially mixed (Garg et al., 2015; Harrison et al., 2012, 2013; Martinsson et al., 2017).

This work aimed to study the variation of AAE in aerosols from different emission sources and to provide a concise compendium of AAE values. In all of the measurements, the state-of-the-art dual-spot aethalometer (model AE33) was used for obtaining $b_{abs}(\lambda)$ at seven wavelengths ranging from the near-UV to near-IR wavelengths (370–950 nm) (Drinovec et al., 2015, 2017). This instrument is widely used for measuring BC concentrations and is well suited for unattended long-term monitoring. Furthermore, it is also used

Table 1
Different Emission Sources and Overview of Measurement Campaigns Under Investigation

Emission source	Fuel	Application type	Reference/information
Shipping	Four different marine oil fuels	Ship engine operated at high and low loads	Aakko-Saksa et al. (2016, 2018)
Buses	Diesel, hybrid and alternative fuels	Controlled driving conditions at depot area	Pirjola et al. (2015), Saarikoski et al. (2017)
Buses	Diesel	In-traffic conditions	Järvinen et al. (2019)
Coal-fired power plant	Coal and coal mixed with wood pellets	Stack gas measurements with and without cleaning	Mylläri (2018), Mylläri et al. (2017, 2019)
Wood burning	Three logwood species and softwood pellets	Modern masonry heater, pellet boiler	Czech et al. (2018), Kanashova et al. (2018), Kortelainen et al. (2018), Reda et al. (2015)
Wood burning	Birch logwood	Sauna stove	Tissari et al. (2019)

in aerosol characterization and source apportionment studies (AE33 has a built-in algorithm to estimate biomass burning contribution of BC via the absorption derived from wavelengths 470 and 950 nm) (Becerril-Valle et al., 2017; Dumka et al., 2018; Healy et al., 2017; Jereb et al., 2018; Martinsson et al., 2017). Thus, it serves as an acceptable instrument reference for measuring the AAE variations.

In this study, the studied emission sources were marine shipping (different marine fuels and engine loads), buses (diesel, hybrid, ethanol, and compressed natural gas-fueled), coal-fired power plant (coal and coal mixed with wood pellets), and wood-burning (masonry heater, pellet boiler, and sauna stove) emissions. Even though the optical properties of aerosols from some of these emission sources have been studied previously, there is a limited amount of information specifically on AAE values. In addition, the information is spread and not harmonious regarding the instrumentation and wavelength pairs used to retrieve the AAE values. In this study, the $b_{\text{abs}}(\lambda)$ were derived consistently by using the same measurement technique and instrumentation, and the data analysis was harmonized. Most of the measurements were performed from fresh emissions during emission tests, thus the AAE values correspond to mainly freshly emitted aerosols and are representative of a given source from a given emission testing protocol.

2. Experimental

2.1. Data Sets

The emission sources studied and data sets utilized in this work are summarized in Table 1. All the data sets used in this study are from measurement campaigns that have already published results. Detailed descriptions of the measurement schemes can be found in the respective publications (Table 1). The terminology used in this study aims to follow the original publications' styles in order to help the reader track the additional information (see Supplementary Information Text S1 for abbreviations and terminology). In the sections below, the experimental measurement schemes are briefly explained for convenience. The reader is encouraged to turn to the references outlined in Table 1 for more details.

2.1.1. Ship Emissions

The exhaust emissions of a marine ship engine loaded with different fuel types and fuel loads were studied under laboratory conditions (Aakko-Saksa et al., 2018, 2016). The measurements were carried out with a 1.6 MW Wärtsilä Vasa 4R32 LN medium-speed engine with a modified configuration at VTT's (Technical Research Centre of Finland) engine laboratory. Four different fuels were tested. Distillate fuel specified as DMB in the international standard ISO 8217, commonly known as marine diesel oil (MDO), had a sulfur content of 0.078% (m/m). Two fuels contained residual type fractions: intermediate fuel oil (IFO) with a sulfur content of 0.38% (m/m) and heavy fuel oil (HFO) with a sulfur content of 2.2% (m/m). A biofuel blend (Bio30) contained 30% of fatty-acid type unesterified biocomponent and 70% of diesel fuel, and its sulfur content was 0.0004% (m/m). Two engine loads were used, 75% and 25%, corresponding to the open sea and near-harbor engine loading conditions, respectively. The exhaust emissions were measured on each marine fuel and engine load for ~60 min. The effect of exhaust pretreatment before the measuring instruments was

studied by using either a thermodenuder (TD) heated to 265 °C or a catalytic stripper (CS) heated to 350°C (Aakko-Saksa et al., 2016; Amanatidis et al., 2018). In addition, a potential aerosol mass (PAM) chamber was used to simulate aerosol aging and secondary aerosol formation (Kang et al., 2007; Lambe et al., 2011). The conditions used in the PAM chamber represented at least two days of aging in the atmosphere (Aakko-Saksa et al., 2016). Comprehensive details of the experimental set up, sampling procedure, physicochemical properties of fuels used, auxiliary instrumentation, and other information are given in Aakko-Saksa et al. (2016, 2018).

2.1.2. Buses

2.1.2.1. Bus Emissions at Depot

The bus exhaust emissions were measured by chasing different types of city buses with a mobile laboratory van “Sniffer” at around 5 m distance at a bus depot area in Helsinki under controlled driving conditions (Pirjola et al., 2015; Saarikoski et al., 2017). The buses were driving a 0.6 km circle, which consisted of two accelerations (from 0 to 25 km/h), two decelerations (back to 0 km/h), and a constant speed (25 km/h) driving periods (cycle repeated 10 times per each bus). In this present study, the average results are presented for acceleration, deceleration, and constant driving conditions (background concentrations were not subtracted). Emissions from 19 individual buses were measured including EURO III, EURO IV, and EEV emission standard class buses with different after-treatment systems (ATS), fuels, and engines. Three of the buses were EURO III diesel buses (no ATS), three EURO IV diesel buses equipped with exhaust gas recirculation (EGR) system along with diesel particle filter (DPF), and 13 were EEV buses. The EEV buses represented different technology choices: two of them were diesel buses equipped with selective catalytic reduction (SCR), four were diesel buses with EGR + DPF, two were diesel-electric hybrid buses with SCR, two were ethanol-fueled (RED95) and equipped with three-way catalysts (TWC), and three buses were fueled with compressed natural gas (CNG) and equipped with TWC. Details of the measurement design and additional information can be found in Pirjola et al. (2015) and Saarikoski et al. (2017).

2.1.2.2. Bus Emissions In-Traffic

Bus exhaust emissions were also measured by chasing different diesel-fueled city buses in-traffic conditions with a mobile laboratory van. The measurements were conducted in an approximately 2.9 km long route (10 min of driving), which was a short part of the local Helsinki region bus line number 550. The buses stopped in seven stops along the route and the route included a 1.7 km long part, which was excluded from other than public transportation. In total, 20 individual buses were tested and these are categorized as follows: EEV (equipped with EGR), EEV retrofits (equipped with either DPF + SCR or EGR + DPF + SCR), and EURO VI (equipped with either DPF + SCR or EGR + DPF + SCR). Detailed descriptions of the measurement scheme and additional information can be found in Järvinen et al. (2019).

2.1.3. Coal-fired Power Plant Emissions

Emissions from a coal-fired power plant were measured from a stack gas under two different cleaning conditions and two different fuel qualities (Mylläri, 2018; Mylläri et al., 2017, 2019). The power plant consists of two coal-fired natural circulation cylinder boilers (363 MW of thermal power). The power plant is located in Helsinki, Finland. The fuel tests were carried out in one of the boilers and the corresponding flue gas ducts, which were boiler specific from the boiler until being released to the atmosphere. The combustion releases flue gases that are cleaned in an electrostatic precipitator, semi-dry flue-gas desulfurization plant (FGD), and fabric filters (FF) before the stack. The measured flue sample was taken from the flue gas duct. The measurement location in the stack was 35 m above sea level. The effect of flue gas cleaning was studied in two different operation conditions: with and without the FGD and FF operating, abbreviated hereafter as “FGD + FF on” or “FGD + FF off”, respectively. In addition to using solely coal as fuel (100% coal), industrial wood pellets mixed with coal were tested (89.5% coal + 10.5% industrial pellet) during the measurement campaign. The emission measurements lasted between 70 and 297 min. Detailed additional information about the measurements, fuel properties, and characterization of the emissions can be found elsewhere (Mylläri, 2018; Mylläri et al., 2017, 2019).

2.1.4. Wood Burning Emissions

2.1.4.1. Masonry Heater and Pellet Boiler

The emissions from wood combustion appliances were studied under laboratory conditions at the ILMARI Laboratory (www.uef.fi/ilmari), Department of Environmental and Biological Sciences, University of Eastern Finland, Kuopio, Finland (Czech et al., 2018; Reda et al., 2015). Two modern wood combustion appliances were studied with different fuels tested. A masonry heater (model HIISI, Tulikivi Ltd, Finland) was applied to produce batch combustion conditions by using three different logwood species (beech [*Fagus sylvatica*], birch [*Betula pubescens*], and spruce [*Picea abies*]) in the experiments. A pellet boiler (model PZ-RL, Biotech Energietechnik GmbH, Austria) was applied to produce continuous combustion conditions by using softwood pellets as fuel. The pellet boiler was operated under factory settings representing efficient modern pellet boiler operation and under unoptimized combustion conditions by reducing the flow of the secondary combustion air to simulate less efficient pellet-fired appliances. With both combustion appliances the combustion experiments lasted for 240 min. During this total combustion period, six batches of wood were burned in the masonry heater. The combustion of each batch lasted for approximately 30 min. After the final batch combustion, the remaining ember was stoked, the secondary air channels were closed and the emissions from the residual char combustion were measured. The total amount of wood burned was approximately 15 kg in each experiment. A few repetitions ($n = 3-8$) were done with each fuel and application tested. More detailed information about the experimental setup, including the properties of the logwoods and instrumentation utilized, and characterization of the emissions can be found elsewhere (Czech et al., 2018; Kanashova et al., 2018; Kortelainen et al., 2018; Reda et al., 2015).

2.1.4.2. Sauna Stove

The emissions from wood burning in sauna stoves (SS) were studied in the small-scale combustion simulator (SIMO) at the University of Eastern Finland (<http://www.uef.fi/en/web/fine/simo>) (Tissari et al., 2019). Two different commercially available sauna stoves were selected for this study (stove 1 and stove 2 here correspond to S1_11 and S6_11 in Tissari et al. (2019), respectively), of which stove 1 was known to emit moderately low PM emissions, whereas the stove 2 was a high PM emitter stove. The combustion period lasted for approximately 90 min during which three batches of wood (total amount 7 kg) were combusted. Three repetitions were done with each stove. Details of the experimental setup and additional information can be found in Tissari et al. (2019).

2.2. Instrumentation

2.2.1. Aethalometer

In all of the measurement campaigns, the dual-spot aethalometer model AE33 (Aerosol d.o.o., Ljubljana, Slovenia) was employed (Drinovec et al., 2015). The aethalometer provides light absorption measurements by the sample aerosol by continuously collecting aerosols in the sampling air stream onto a filter tape. As light-absorbing aerosols are deposited onto the filter, the filter gradually gets laden with aerosols and the spots on the filter where the aerosols are deposited get darker; the attenuation (ATN) of light through the filter increases. The amount of light absorbing aerosols is calculated from the rate of change of the attenuation (ΔATN) of the light transmitted through the filter. Two sample spots, with different flow rates of aerosol accumulation, and a reference spot are used for the calculation of aerosol light absorption coefficients ($b_{\text{abs}}[\lambda]$) (equation (17) in Drinovec et al. (2015)). In model AE33, the filter-loading effect compensation parameter (k) is used to correct the $b_{\text{abs}}(\lambda)$ results automatically in real-time (Drinovec et al., 2015, 2017). The measurements are done at seven different wavelengths (370 nm, 470 nm, 520 nm, 590 nm, 660 nm, 880 and 950 nm). The instrument reports the measurements in units of equivalent BC (eBC) mass concentrations as data output values by using specific mass absorption cross-section (MAC) and filter multiple scattering parameter (C) values in the calculations. The AE33 sampling parameters and settings (including C values) used in the different measurement campaigns are summarized in Table S1, and the employed default mass absorption cross-section values are shown in Table S2. In this study, the AE33's measured loading compensated eBC (λ) concentrations were simply converted to $b_{\text{abs}}(\lambda)$ as shown in Equation 1.

$$b_{\text{abs}}(\lambda) = \text{eBC}(\lambda) * \text{MAC}(\lambda) \quad (1)$$

In the majority of the studies presented in Table 1, the aethalometer was used to only report the eBC mass concentration at 880 nm wavelength. The variation of AAE has been covered previously only in sauna stove emissions (Tissari et al., 2019).

2.3. Data Handling and Central Points

The AAE values were calculated by using either two wavelengths (Equation 2, $AAE_{470/950}$) or from the slope of least-square fit of the logarithm of $b_{abs}(\lambda)$ versus the logarithm of seven wavelengths ($AAE_{370-950}$). It has been previously shown, that the method used to calculate the AAE values may impact the results and even affect the interpretation (Lack & Cappa, 2010). Also, as mentioned in the introduction, the wavelengths used in calculations may affect the derived absolute value of AAE.

$$AAE_{470/950} = - \frac{\ln\left(b_{abs}(470 \text{ nm}) / b_{abs}(950 \text{ nm})\right)}{\ln(470 / 950)} \quad (2)$$

We investigated the AAE values by using both the two wavelength and seven wavelength fitting methods, which are abbreviated herein as $AAE_{470/950}$ and $AAE_{370-950}$, respectively. The main emphasis in the interpretation of results is given for the two wavelengths calculation method. The wavelengths used here were 470 and 950 nm. These were selected by following the suggestion of Zotter et al. (2017) and since this wavelength pair is implemented in the online source apportionment of the AE33. It is likely, that these wavelength pairs will be the most common ones used in future source apportionment studies (i.e., in the Aethalometer model). Thus, the seven wavelength fitting $AAE_{370-950}$ results are given here mainly as supplementary data.

The presented AAE values were retrieved from the whole measurement period averaged $b_{abs}(\lambda)$ coefficients. However, the standard deviations (SD) assigned to these average AAE values were obtained by calculating the AAE values by using the high time resolution of measurement and by taking the standard deviation from these (prior to this, most 1 s $b_{abs}[\lambda]$ measurements were first averaged to 60 s, Table S1). When applicable, these average AAE values were further averaged according to the number of repetitions (e.g., in wood combustion experiments, $n = 3-8$) or a number of individual experiments (e.g., bus route driven, $n = 6-22$), and in those cases, the AAE average and standard deviations were reported based on these. This was the calculation process used in the majority of the campaigns and the overall results are presented based on this procedure. The only exception was the AAE values retrieved from the bus emission measurements performed at the depot area. There, the data handling was based on the way it was done in the work by Pirjola et al. (2015), where it was necessary to keep the 1 s $b_{abs}(\lambda)$ time resolution to capture the different driving cycle phases. There, the AAE values were retrieved based on the averaged $b_{abs}(\lambda)$ from the 10 repetitions performed for individual buses. These AAE values were then further averaged according to the number of buses within each emission class.

Since AAE is an invariant unitless parameter (Equation 2), the various emission processing setups/settings utilized in the emission measurements do not affect the AAE values in the same way as they affect quantitative mass concentration measurements as the potential losses are likely similar for all $b_{abs}(\lambda)$. However, even though AAE is not per se affected by for example, the losses and uncertainties in the dilution ratios (which are discussed in the referenced publications, Table 1) in the same way as the absolute $b_{abs}(\lambda)$, the experimental conditions might still affect directly to the derived AAE values. Particulate and gaseous emissions and thus the AAE results are subject to the combustion and experimental conditions used in the different appliances. As practical emission measurements are notoriously challenging to be performed, the combustion efficiency and dilutions used in the experiments likely have an effect on the AAE results due to, e.g., condensation or volatilization of organics and possibly variable EC/OC ratios, which may affect the absorption in short wavelengths (Garg et al., 2015; Martinsson et al., 2015; Pokhrel et al., 2016; Robinson et al., 2007). Thus, the reader should be aware that the AAE results are representative to some extent of the set instrumentation and sampling systems used in the emission measurements and are not necessarily solely representative of the given emission sources, i.e., the AAE values are also affected by the experimental settings used in the given emission tests.

2.4. Estimation of the AAE Uncertainty

In general, the $b_{\text{abs}}(\lambda)$ measurement uncertainty of the aethalometer has been estimated to be in the range of $\pm 10\%$ to $\pm 35\%$ (Di Biagio et al., 2017; Healy et al., 2017; Zanatta et al., 2016), however, there is not much information about the uncertainty of the AAE. Here, the uncertainty of the $\text{AAE}_{470/950}$ (δAAE) was estimated by using Equation 3. The detailed derivation of this formula can be traced in the supplement Text S2. In Equation 3 $\delta\Delta\text{ATN}$ is the uncertainty in the measured rate of change in attenuation and δk is the uncertainty in the wavelength-dependent compensation parameter.

$$\delta\text{AAE} = \sqrt{\left(\left(\frac{\delta\Delta\text{ATN}}{\Delta\text{ATN}_{470}} \right)^2 + \left(\frac{\delta\Delta\text{ATN}}{\Delta\text{ATN}_{950}} \right)^2 \right) + \frac{1}{2} \left(\left(\frac{k_{470}\delta\Delta\text{ATN}}{1 - k_{470}\text{ATN}_{470}} \right)^2 + \left(\frac{k_{950}\delta\Delta\text{ATN}}{1 - k_{950}\text{ATN}_{950}} \right)^2 \right) + \left(\frac{\text{ATN}_{470}\delta k_{470}}{1 - k_{470}\text{ATN}_{470}} \right)^2 + \left(\frac{\text{ATN}_{950}\delta k_{950}}{1 - k_{950}\text{ATN}_{950}} \right)^2} \quad (3)$$

Some fundamental conclusions can be drawn from this formula. The term $\left(\frac{\delta\Delta\text{ATN}}{\Delta\text{ATN}_{470}} \right)^2 + \left(\frac{\delta\Delta\text{ATN}}{\Delta\text{ATN}_{950}} \right)^2$ shows that the smaller ΔATN is, the higher is the AAE uncertainty. This means for instance that at constant $b_{\text{abs}}(\lambda)$ values the shorter the time step Δt is, the larger is the AAE uncertainty. It also means that at a constant Δt the larger the ΔATN is, the lower is the AAE uncertainty which means that the higher the $b_{\text{abs}}(\lambda)$ is the lower is the uncertainty of its AAE. In the rest of the terms in the square root of Equation 3 there are the wavelength-dependent divisions by $1 - k\text{ATN}$. Typically, the compensation parameter $k > 0$ and $1 - k\text{ATN}$ decreases with increasing ATN for both wavelengths, and consequently the AAE uncertainty increases. This suggests that for heavily loaded filters AAE is more uncertain than for fresh filters. The last two terms in Equation 3 strengthen this effect further by the multiplication of ATN with the uncertainties of the compensation parameters. Furthermore, it should be noted that at high ATN, ΔATN itself becomes smaller and hence the uncertainty at high filter loadings is related to the instrument detection (see Text S3).

To get quantitative estimates of δAAE , the uncertainties $\delta\Delta\text{ATN}$, δk_{470} , and δk_{950} are needed. We did not directly measure $\delta\Delta\text{ATN}$ so we used the average of the values presented in Table 2 of Backman et al. (2017). Those noises were for 5-min time steps. To estimate $\delta\Delta\text{ATN}$ at shorter or longer time steps we used Equation 4. For future studies, campaign-specific particle-free zero air measurements would be beneficial.

$$\delta\Delta\text{ATN}(\Delta t) = \frac{\delta\Delta\text{ATN}(\Delta t = 5 \text{ min})}{\sqrt{\Delta t(s) / 300 \text{ s}}} \quad (4)$$

The compensation parameter uncertainties were calculated as the standard deviations of k_{470} and k_{950} in our data sets. The relative standard deviation of the compensation parameter in the campaigns was on average $k_{470} = 22\%$ and $k_{950} = 37\%$. The averages of k_{470} and k_{950} were used in Equation 3, ΔATN_{470} was set to vary from “noisy” 0.01 to “optimal” 1.0 and the corresponding ΔATN_{950} was calculated by using Equation 5. In Equation 5, $\text{AAE} = 1.0$ was used in all cases for simplicity. The ATN_{470} was let to vary in the range of 0%–100% and ATN_{950} in the range of 0%–50%. The resulting δAAE were plotted for time steps from 1 s to 120 min.

$$\Delta\text{ATN}_{950} = \frac{\Delta\text{ATN}_{470}}{(950 / 470)^{\text{AAE}}} \quad (5)$$

The overview of the estimated uncertainty of AAE in the measurements conducted in this study can be seen in Figure 1. As mentioned above, the smaller the ΔATN is, the higher the δAAE is. In the “optimal” case the $|\delta\text{AAE}/\text{AAE}|$ varies approximately in the range of 1%–45% depending on the averaging time (Figure 1a), whereas in the “noisy” case the $|\delta\text{AAE}/\text{AAE}|$ varies in the range of 53%–4,366% (Figure 1c). The averaging time plays a central role in the magnitude of δAAE . In Figure 1d the effect of the uncertainty in compensation parameter is demonstrated by using relative uncertainties of 5%, 25%, and 50% in both k_{470} and k_{950} . The larger the δk is, the larger is the δAAE for the heavily loaded filter (more apparent for low ΔATN).

Table 2
The Range of Estimated $AAE_{470/950}$ Relative Uncertainties in the Different Emission Measurements

Source	$\Delta ATN_{470} = 1.0$			$\Delta ATN_{470} = 0.1$			$\Delta ATN_{470} = 0.01$		
Shipping	1 min	8 min	62 min	1 min	8 min	62 min	1 min	8 min	62 min
	6–36	2–36	1–36	56–67	20–41	7–36	~565	199–202	72–80
Buses at depot	1 s	9 s	70 s	1 s	9 s	70 s	1 s	9 s	70 s
	44–46	15–21	5–16	~437	~146	52–54	~4366	~1456	~522
Buses in traffic	1 min		10 min	1 min		10 min	1 min		10 min
	6–12		2–10	56–57		18–20	~564		~179
Power plant	1 min	70 min	297 min	1 min	70 min	297 min	1 min	70 min	297 min
	6–28	1–28	0–27	56–63	7–28	3–28	~564	67–73	33–43
Masonry heater	1 min	30 min	240 min	1 min	30 min	240 min	1 min	30 min	240 min
	6–41	1–40	0–40	56–69	10–42	4–40	~565	103–110	36–54
Sauna stove	1 min		90 min	1 min		90 min	1 min		90 min
	6–10,289		1–10,289	56–10,289		6–10,289	564–10,304		59–10,289

Note. The $|\delta AAE/AAE|$ in percentages are presented for three different ΔATN_{470} values and for different campaign specific averaging times. The presented relative uncertainty range corresponds to minimum–maximum in the ATN range, except few cases, are rounded to a single value. The same information is presented as plots in Figure S1.

As mentioned in the previous sections, in this work the $b_{abs}(\lambda)$ were averaged at as high time resolution as possible prior to deriving the AAE values. Typically, this meant from few minutes to tens or hundreds of minutes, thus the δAAE was improved even if the original raw data had periods with low ΔATN . The campaign-specific estimates of δAAE and $|\delta AAE/AAE|$ are presented in Figure S1 and Table 2. These estimates are presented for the high time resolution and for the used averaging times. The very high maximum uncertainty in the case of the sauna stove emissions was due to the reason that the tape advance threshold was disallowed during the burn cycle (Tissari et al., 2019), which caused the attenuation rise to high values (on average to $ATN_{470} \approx 280$).

3. Results and Discussion

3.1. General Characteristics of AAE Variation from Different Emission Sources

Substantial variation was observed in the AAE values derived from the different emission sources under investigation in this study. An overview of results is shown in Figures 2, 3, S2, and Table S3. On average, the $AAE_{470/950}$ values ranged from -0.2 ± 0.7 to 3.0 ± 0.8 ($AAE_{370-950}$ from 0.1 ± 0.6 to 2.7 ± 0.7) within the studied fresh emission sources (Figure 2 and Table S3). Both of these extremes were observed for ethanol-fueled bus emissions, which, to the best of our knowledge, have not been previously addressed in terms of AAE variation. Even when excluding these results from the investigation of $AAE_{470/950}$ variation, the observed deviation is substantial; from -0.1 ± 2.1 to 2.0 ± 0.1 (for $AAE_{370-950}$ from 0.4 ± 1.1 to 2.1 ± 0.0). The second-lowest AAE was observed for coal-fired power plant emissions (with FGD + FF on) and the second highest for HFO fueled ship engine emissions (Figure 2).

The high correlation ($R^2 = 0.95$) between the $AAE_{370-950}$ and $AAE_{470/950}$ results indicated fairly good agreement between the two different AAE calculation methods (see Section 2.3) (Figure 3). Although different wavelength ranges were used in these calculations (namely the lowest wavelengths selected, either 370 nm or 470 nm), the overall trend in the AAE results was similar (Figure 3). For example, similar to the $AAE_{470/950}$ results, the lowest $AAE_{370-950}$ values were observed for the alternative-fueled buses and for the coal-fired power plant emissions (e.g., Figure S2). Also, the highest $AAE_{370-950}$ values were observed in ship engine emissions and in wood combustion emissions, if excluding the alternative-fueled buses from results (Figure S2 and Table S3). In the data sets studied in this work, the main differences in the absolute $AAE_{470/950}$ and $AAE_{370-950}$ values were typically observed when the $b_{abs}(\lambda)$ values were low (illustrated in Figure 3 as

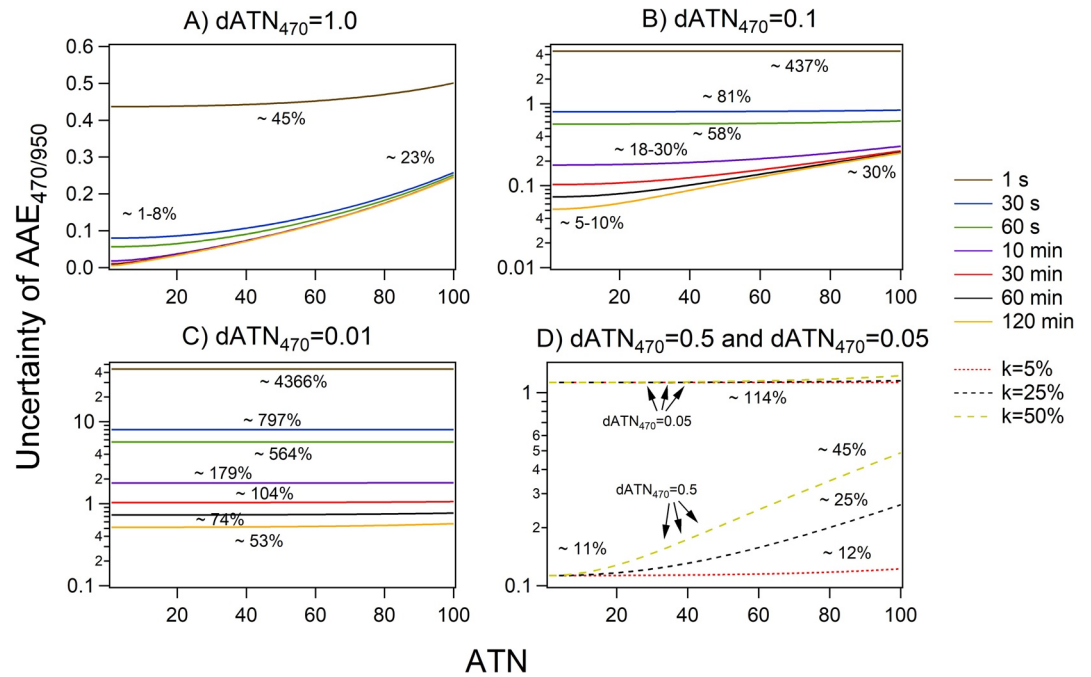


Figure 1. The estimated uncertainty of $AAE_{470/950}$ as a function of attenuation. In (a), (b), and (c) different ΔATN values (0.01, 0.1, and 1.0) were tested as well as different averaging times (from 1 s to 120 min). In (d) the effect of relative uncertainty in k values was tested for two different ΔATN values (for 1 min averaging time). The relative uncertainties of AAE are marked in the plots. AAE, Absorption Ångström exponent; ATN, attenuation.

$b_{\text{abs}}(880 \text{ nm})$ colored markers). As can be seen in Figure 3, the greatest differences between the $AAE_{470/950}$ and $AAE_{370-950}$ results were accompanied by the high deviation in AAE values and low $b_{\text{abs}}(880 \text{ nm})$ levels in emissions. Statistically, the mean bias error was 0.03, the root mean square error was 0.14 and the normalized root mean square error was 12% when calculated by using all the data presented in Table S3. Consequently, the difference between the $AAE_{370-950}$ and $AAE_{470/950}$ results can be considered to being quite small.

Results from different campaigns are next covered in detail. In the following sections, first, a general overview of aerosol emission results is given based on the information provided in the previous publications (Table 1), and then the focus is shifted toward the AAE results. As mentioned in Section 2.3, the main emphasis on the interpretation of the results is now set on the $AAE_{470/950}$. The $AAE_{370-950}$ results are presented only when deemed necessary.

3.2. AAE Results from the Ship Engine Exhaust Emissions

The exhaust emissions measured from the ship engine operated with different marine fuels and engine loads showed some particularly interesting features. As shown previously in Aakko-Saksa et al. (2016, 2018), particulate matter (PM), organic carbon (OC) and BC emissions were generally higher at engine load 25% than at load 75% for the different fuels tested. The observed trend in BC emissions was consistent with previous observations (Lack & Corbett, 2012), that is, increasing emissions with decreasing engine load (Aakko-Saksa et al., 2016). The BC emissions were the highest at high and low loads when HFO and IFO were used as fuels, respectively (Aakko-Saksa et al., 2016). The corresponding $b_{\text{abs}}(\lambda)$ levels are presented in Figure S3. Overall, the emissions from high sulfur content fuels (HFO and IFO) also contained the highest amounts of metals (including e.g., V, Fe, Ca, and Ni), polyaromatic hydrocarbons (PAHs), and low volatility organic compounds (Aakko-Saksa et al., 2016, 2018).

Considering the variation of $AAE_{470/950}$ values, the highest $AAE_{470/950}$ values were observed for the HFO fuel and the lowest for the MDO fuel at both high and low engine loads (Figures 2 and S4). For the HFO fuel, the $AAE_{470/950}$ values were 2.0 ± 0.1 and 1.6 ± 0.0 under high and low loads, respectively. With the other

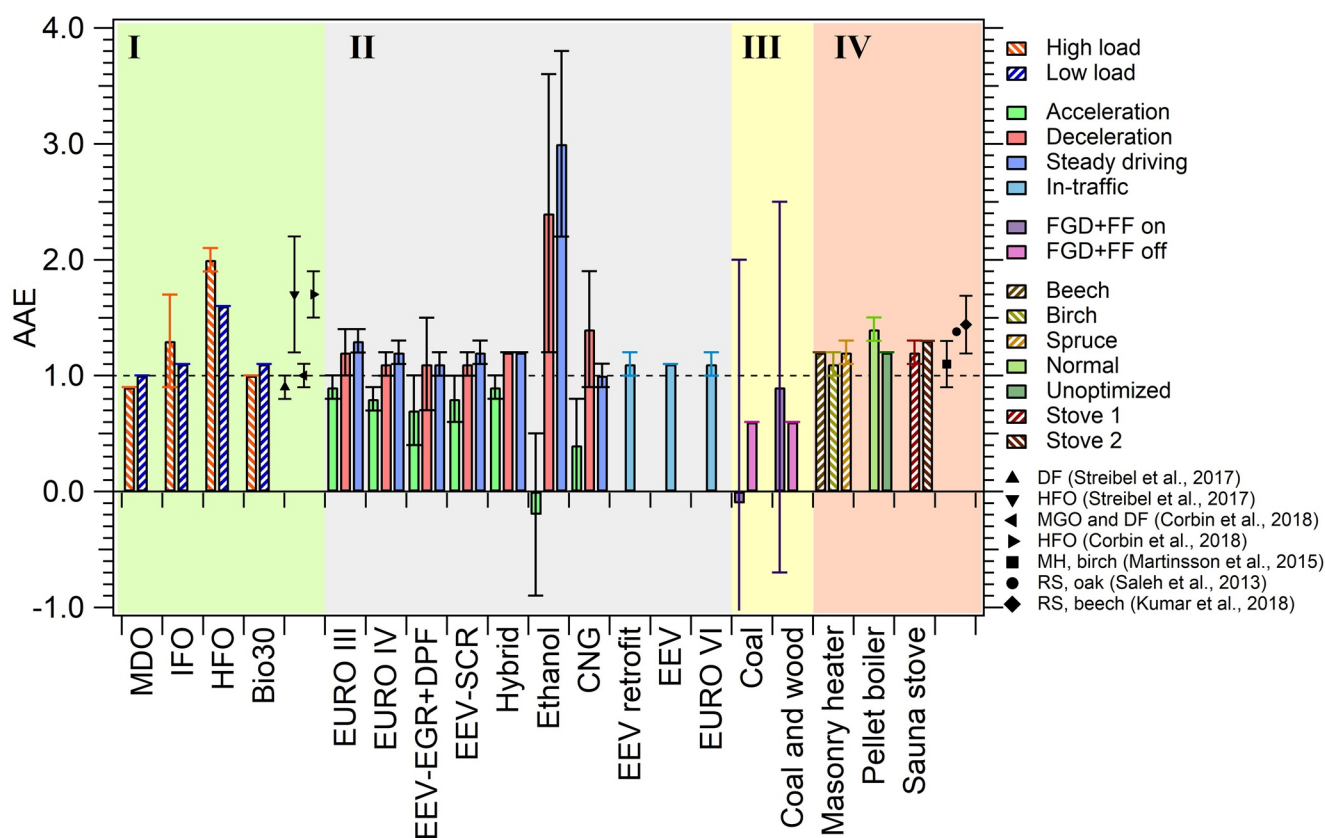


Figure 2. The variation of AAE_{470/950} values (average ± standard deviation) from different emissions sources: I) shipping II) buses III) power plant and IV) wood burning emissions (different emission sources are differentiated based on the colored background boxes). The bar colors are identified in the right-side legends. The abbreviations and experiments have been described in Section 2.1. The common threshold value AAE = 1 for BC is shown in the plot as a dashed line for reference. Previously reported literature AAE values, shown as different marker symbols, are presented in the plot and identified in the legends. AAE, Absorption Ångström exponent; DF, distillate fuel; HFO, heavy fuel oil; MGO, margin gas oil; MH, masonry heater; RS, residential stove.

fuels tested, the AAE_{470/950} values were in the range of 0.9–1.1, except with IFO, which had an AAE_{470/950} of 1.3 ± 0.4 when the engine was operated at high load. A similar difference between the “pure” distillate fuels and HFO has been observed also previously (Figure 2) (Corbin et al., 2018; Mueller et al., 2015; Streibel et al., 2017), for example, Streibel et al. (2017) observed AAE values to vary from 1.2 to 2.5 in emissions from HFO 180 (1.6% S content) fueled engine, whereas in emissions from an engine operated with distillate fuel (DIN EN 590) the AAE value was ~1. It is plausible, that the relatively high PAH and metal content of the HFO and IFO emissions (see above) are explaining the observed relatively high AAE values (Aakko-Saksa et al., 2016). Both components may enhance the light absorption at the low visible wavelengths, therefore explaining the observed AAE > 1. It should be noted that only HFO is clearly distinguishable from pure BC under both high and low engine loads.

The effect of exhaust emissions treatment by using a thermodenuder or a catalytic stripper did not change the observed AAE_{470/950} values dramatically (Figure 4). This was especially the case when the engine was operated at low load (Figure 4b). At high engine load, the AAE_{470/950} values decreased slightly after treatment. However, the difference between no-treatment and pretreatment was almost within the standard deviations (Figure 4a). This shows that the AAE values are more sensitive to fuel type than what is removed by thermodenuding or catalytic stripping. Consequently, this indicates that even if the BC particles were coated by volatile organics, the effect of coating was not dramatic in terms of the spectral dependence of light absorption. These pretreatment results also point toward the conclusion that the observed high AAE_{470/950} values in the case of HFO emissions were likely due to the metal content and/or non-volatile light-absorbing organics since the pretreatment processes utilized here only remove the volatile and some sulfur-containing species (Aakko-Saksa et al., 2016; Amanatidis et al., 2018). Nevertheless, these pretreatment experiments were unfortunately short in duration (13–30 min), and could warrant further investigation.

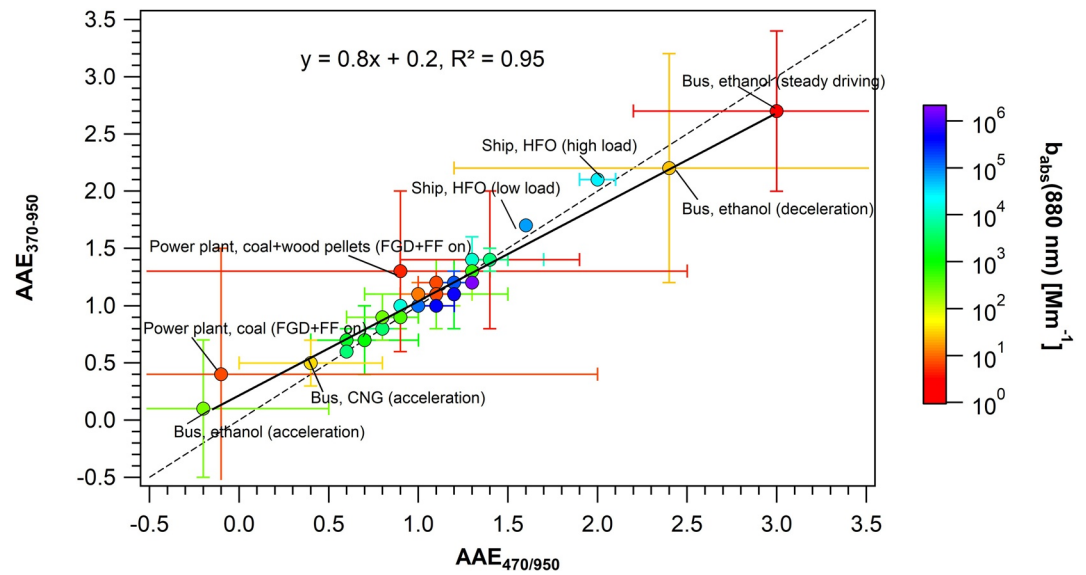


Figure 3. Relationship between the average (\pm standard deviation) $AAE_{370-950}$ and $AAE_{470/950}$ results. The markers are colored based on the logarithm of $b_{abs}(880 \text{ nm})$ measured in emissions. Few of the markers in the extreme ranges are identified in the plot for illustrative purposes (for abbreviations see e.g., Section 2.1). The solid black line shows the linear regression analysis fit. The dashed black line represents a 1:1 relation.

The effect of atmospheric aging was simulated via PAM chamber experiments by applying conditions representative of at least two days of aging (Aakko-Saksa et al., 2016). The results from these experiments should be considered tentative due to the short measurement periods utilized in some of the experiments (8–56 min). In general, no distinct trend was observed on the effect of simulated atmospheric aging (Figure 4). When the engine was operated at low load, the $AAE_{470/950}$ values were similar in fresh and aged emissions for all fuels except for HFO (Figure 4d). With HFO, the $AAE_{470/950}$ was 1.3 ± 0.0 and 1.8 ± 0.1

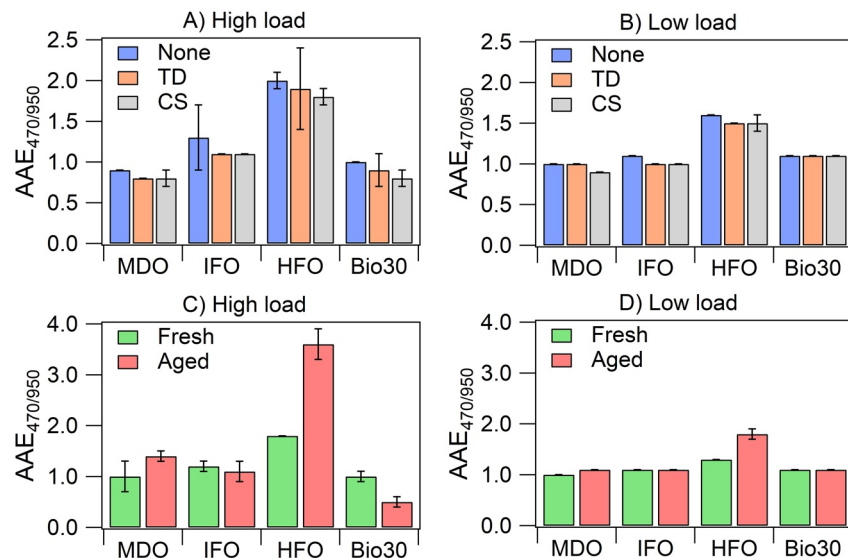


Figure 4. The effect of pretreatment and aging on the $AAE_{470/950}$ values for different fuels and engine loads tested in the ship engine emissions. The upper panel plots (a) and (b) represent the pretreatment results. The lower panel plots (c) and (d) represent the PAM chamber results, fresh being the situation when the voltages were off and aged the situation with voltages on. *Note.* the difference in y-axis scales between the upper and lower panels. AAE, Absorption Ångström exponent; CS, catalytic stripper; TD, thermodenuder.

in fresh and aged emissions, respectively. Similarly, with HFO at high load, the $AAE_{470/950}$ increased from 1.8 ± 0.0 to 3.6 ± 0.3 between the fresh and aged aerosols. For the other fuels tested at high load, no equally clear trend was found in $AAE_{470/950}$ (Figure 4c). Upon aging, the BC particles likely become coated with the co-emitted pollutants and grow in size due to oxidation and subsequent condensation by initially gas-phase pollutants. Based on these experiments it seems that at high engine load, the effect of aging on AAE values depends greatly on the fuel used.

3.3. AAE Results from the Bus Chasing Experiments

3.3.1. Depot Area

The bus chasing experiments conducted at the bus depot allowed for the investigation of the effect of different driving conditions on the AAE values derived from bus exhaust emissions. As shown in Pirjola et al. (2015) and Saarikoski et al. (2017), the highest BC and organics emissions were observed during the acceleration phase for nearly all bus types and fuels tested, whereas the lowest emissions were mainly observed during steady driving conditions. In general, the emissions were the highest for older bus types (e.g., EURO III and EURO IV) and decreased toward the newer bus types (e.g., EEVs and hybrid) and alternative fuels (Pirjola et al., 2015). In addition, the total particle number (PN) concentration showed a similar trend: the highest PN concentrations were observed during the acceleration phase and more so with older type buses, whereas the lowest PN concentrations were observed during steady driving and with alternative fuel buses (Pirjola et al., 2015). The corresponding $b_{\text{abs}}(\lambda)$ levels for different bus types and driving conditions are presented in Figure S5.

Interestingly, AAE was also observed to vary almost systematically during different driving conditions (Table S3). The lowest $AAE_{470/950}$ values were observed during acceleration and the highest during steady driving (Figure 2). For diesel-fueled and hybrid buses, the $AAE_{470/950}$ values were on average 0.8 ± 0.1 , 1.1 ± 0.1 , and 1.2 ± 0.1 during acceleration, deceleration, and steady driving conditions, respectively. Considering the overall results, the $AAE_{470/950}$ was in the range of 1.0 ± 0.3 for the diesel and hybrid buses. This is in agreement with the literature values of AAE measured from traffic and diesel engine emissions (Blanco-Alegre et al., 2020; Guo et al., 2014; Kirchstetter et al., 2004; Olson et al., 2015). However, the observed trend of AAE variation for the different driving conditions is particularly interesting and, to our knowledge, has not been addressed previously.

As shown in Pirjola et al. (2015), the bimodal shape of the particle number size distributions was observed for all diesel-fueled and hybrid buses. The smaller nucleation mode peaked at around 10 nm and the “soot mode” at 60–80 nm (mobility diameter) (Pirjola et al., 2015). During the acceleration phase, the soot mode dominated the particle number concentrations from most of the diesel-fueled and hybrid buses, whereas during deceleration and steady driving conditions the nucleation mode was the dominant size. In other words, the particle size distribution was leaning toward larger particle sizes during the acceleration phase and toward smaller sizes during deceleration and steady driving. Assuming that the light-absorbing particles were primarily externally mixed or internally mixed with only thin coating in these fresh exhaust emissions, the behavior of the observed AAE trend could be explained by different size distributions and/or particle morphology. However, as shown in Pirjola et al. (2015), the organic species dominated PM_{10} composition during acceleration, whereas during steady driving the BC dominated the PM_{10} composition. In view of this, it would be more plausible that during the acceleration phase the BC particles become more coated than during steady driving. Therefore, the fact that the AAE is varying between different driving phases might be induced by both the differentiating BC particles sizes and morphology, and/or co-emitted organics resulting in coated BC particles preferably during acceleration. It should be noted that the difference in AAE values between the driving phases might be affected also by the difference in non-exhaust-derived particles (e.g., particles originating from brake pads/disk, tires, and asphalt).

It is difficult to address which of these phenomena are exactly causing the observed AAE variation. Assuming that the size distributions presented in Pirjola et al. (2015) are indicative of BC core sizes, then the observations could be explained by following the Mie core-shell modeling studies (Gyawali et al., 2009; Lack & Cappa, 2010; Virkkula, 2020). As mentioned in the introduction, in general, the AAE decreases when the BC core size increases ($> \sim 100$ nm). Therefore, the predominance of the larger particle sizes during the

acceleration phase in comparison to other driving conditions might be the reason for the observed AAE trend during different motorcycle phases. When comparing to previous studies, Guo et al. (2014) measured emissions from a diesel-fueled light-duty truck running on a chassis dynamometer and observed $AAE_{405/532}$ to be on average 1.84 ± 0.32 under high-speed driving period (70 km/h) and $AAE_{405/532} = 1.16 \pm 0.27$ under other driving periods in the applied transient cycle. Even though it is not explicitly addressed in their study, one can see in their plotted AAE values and vehicle speeds that the AAE values are generally rising when accelerating and AAE values dropping during deceleration. Accordingly, during the short “constant speed” driving periods in the Guo et al. (2014) study run transient cycle, the AAE would be presumably higher than during the acceleration/deceleration phases, which is similar to what was observed in our results.

For the alternative fuel buses (ethanol and CNG), the variation of AAE deviated from the observations of conventional diesel and hybrid buses (Figure 2). In general, the measured BC emissions were significantly lower for the alternative fuel buses when compared to the diesel-fueled buses (Pirjola et al., 2015). The BC concentrations were mostly close to the background levels. Only during the acceleration phase, the BC emissions were similar between the ethanol-fueled buses and some of the diesel buses (see also Figure S5) (Pirjola et al., 2015). Nevertheless, during the acceleration phase the observed $AAE_{470/950}$ was on average -0.2 ± 0.7 for ethanol buses ($AAE_{370-950} = 0.1 \pm 0.6$). The chemical composition analysis results revealed, that during the acceleration phase BC and organics accounted for 75% and 25% of the PM_1 emissions, respectively (Pirjola et al., 2015; Saarikoski et al., 2017). In contrast to the soot mode observed in the particle number size distributions for diesel-fueled buses, the second mode observed for ethanol buses peaked at much smaller sizes (at 20–30 nm) (Pirjola et al., 2015). The particle number size distribution for ethanol-fueled buses was dominated by the 10 nm sized particles during the acceleration phase (Pirjola et al., 2015). Considering these differences in chemical composition and size distribution between the diesel buses and ethanol buses, it is not surprising that also the AAE values were different (Figure 2).

However, the reasons for why negative $AAE_{470/950}$ (or very low $AAE_{370-950}$) values were observed for ethanol-fueled buses is cumbersome to assess. It should be mentioned that the ethanol-fueled buses also used different lubrication oil and after-treatment system (Pirjola et al., 2015), so the AAE differences are not necessarily related solely due to the difference in fuels and how they combust. Other than during the acceleration phase, the $b_{abs}(\lambda)$ levels were low (close to background levels) and the derived AAE values have high uncertainty. If taking into account only $b_{abs}(\lambda)$ data during which the $b_{abs}(880 \text{ nm})$ values were equal or greater than the 40th percentile of the entire chasing period $b_{abs}(880 \text{ nm})$ values, then the derived average $AAE_{470/950}$ mostly decreased. In ethanol bus emissions the $AAE_{470/950}$ dropped from 2.4 ± 1.2 to 1.5 ± 0.4 upon deceleration and from 3.0 ± 0.8 to 1.3 ± 0.1 upon steady driving but stayed similar during the acceleration phase (change from -0.2 ± 0.70 to -0.1 ± 0.6 , or for $AAE_{370-950}$ from 0.1 ± 0.6 to 0.1 ± 0.5). In CNG bus emissions, the changes were as follows: from 0.4 ± 0.4 to 0.2 ± 0.5 (acceleration), from 1.4 ± 0.5 to 0.7 ± 0.5 (deceleration), and from 1.0 ± 0.1 to 0.7 ± 0.2 (steady driving), when taking into account only the ≥ 40 th percentile data. Further research eliminating ambient influence would have to be conducted in laboratory conditions to study the effect of alternative fuels in greater detail.

3.3.2. In-traffic Bus Route

The results obtained from the in-traffic bus chasing experiments were similar to the results obtained at the bus depot (considering that all buses were diesel-fueled, Figure 2). The corresponding $b_{abs}(\lambda)$ levels for EURO VI, EEV retrofit, and EEV buses are shown in Figure S6. The derived $AAE_{470/950}$ values in these in-traffic chasing experiments were 1.1 ± 0.1 . In general, the $AAE_{470/950}$ values were similar between the different bus classes (Figure 2). These observed AAE values are in line with the above-mentioned observations (Section 3.3.1) considering that the bus route consisted of both steady driving and start-and-stop driving phases. However, the effect of background and emissions from other vehicles may impact the results obtained from these in-traffic chasing experiments to a greater extent than during the bus depot measurements. Especially with EURO VI and EEV retrofit buses, the measured PM and BC concentrations were low and close to background concentrations (Järvinen et al., 2019). Nevertheless, it appears that regardless of the after-exhaust treatment system or bus emission class, the AAE is generally close to ~ 1 for all diesel-fueled buses. For example, considering all the diesel-fueled buses from the two campaigns (depot

and in-traffic), the average $AAE_{470/950}$ was 1.0 ± 0.2 , which is in the range of typical AAE values observed in traffic dominated environments (Blanco-Alegre et al., 2020; Herich et al., 2011; Kirchstetter et al., 2004; Resquin et al., 2018).

3.4. AAE Results from the Flue-gas of Coal-fired Power Plant

In general, as shown in Mylläri (2018), the emissions of PM, PN, and BC were significantly higher when the desulfurization plant cleaning was bypassed (“FGD + FF off”) when compared to the normal operating conditions (“FGD + FF on”) of the coal-fired power plant. For example, the BC emissions were roughly 240–800 fold higher during the “FGD + FF off” than during the “FGD + FF on” situation (Mylläri, 2018; Mylläri et al., 2019). During the “FGD + FF off” operation, the BC emissions were 3-fold higher when the coal and wood pellet mixture was used in comparison to using simply coal as fuel (Mylläri, 2018). In contrast, during the “FGD + FF on” operation, the BC emissions were similar for both coal and the mixture of coal and wood pellet (Mylläri, 2018).

The $AAE_{470/950}$ values showed substantial variation during the “FGD + FF on” operation (Figure 2). The measured $b_{\text{abs}}(\lambda)$ levels were rather low and noisy at all wavelengths during the “FGD + FF on”, whereas during the “FGD + FF off” operation the $b_{\text{abs}}(\lambda)$ levels were more consistent and higher (Figures S7 and S8). Consequently, the variation in $AAE_{470/950}$ values was higher during the “FGD + FF on” operation than during the “FGD + FF off” operation. No common trend in average $AAE_{470/950}$ could be identified between the different fuels and operation conditions. When coal was used as fuel, the $AAE_{470/950}$ value increased from -0.1 ± 2.1 to 0.6 ± 0.0 when the cleaning was bypassed (for $AAE_{370-950}$ from 0.4 ± 1.1 to 0.7 ± 0.1), whereas in coal + wood pellet experiments the $AAE_{470/950}$ value decreased from 0.9 ± 1.6 to 0.6 ± 0.0 when the cleaning was bypassed (for $AAE_{370-950}$ from 1.3 ± 0.7 to 0.6 ± 0.0).

Most likely, the reason for these $AAE_{470/950}$ observations is related to the differentiating PM composition and particle sizes between the different desulfurization plant operational situations and to different fuel properties. As shown in previous studies from the same measurements, the particles were generally larger during the “FGD + FF on” situation when compared to the “FGD + FF off” situation (Mylläri, 2018). Detailed characterization of the particles revealed, for example, that during the “FGD + FF off” situation soot particles could be identified, whereas during the “FGD + FF on” situation soot particles were not distinctly identified from transmission electron microscope (TEM) images of particle samples (Mylläri, 2018; Mylläri et al., 2019). Hence, the $AAE < 1$ values might be due to both the efficient removal of soot particles and generally larger particle sizes. As mentioned before, when the BC particle core size increases, the AAE decreases toward negative values (Gyawali et al., 2009; Lack & Cappa, 2010; Virkkula, 2020). Based on the TEM images and energy dispersive X-ray spectrometer (EDS) analysis results from the emissions (Mylläri, 2018), it seems likely that the observed low AAE values and $b_{\text{abs}}(\lambda)$ levels are mainly indicative of the chemical composition of the emitted particles. As reviewed in Mylläri (2018), the particles after the “FGD + FF on” have been observed to contain largely chemical components used in reagents in the desulfurization plant (e.g., inorganic salts such as CaSO_4 and NaCl). Therefore, it is not surprising that the measured $b_{\text{abs}}(\lambda)$ levels were low and noisy, and that the retrieved AAE values were highly variable during “FGD + FF on”.

In summary, when the coal-fired power plant is operating normally (“FGD + FF on”), the $b_{\text{abs}}(\lambda)$ levels are relatively low and the variation of AAE is large. It would be only under malfunction circumstances in the desulfurization plant when the $b_{\text{abs}}(\lambda)$ levels would be high and the AAE in emissions roughly 0.7 ± 0.1 (Table S3). Unfortunately, we did not find any recent literature on AAE values from fresh coal-fired power plant exhaust to compare our results to. However, if considering the AAE results reported for coal combustion originating aerosols from the residential sector (Bond et al., 2002; Goetz et al., 2018; Liu et al., 2018; Olson et al., 2015; Sun et al., 2017; Yan et al., 2017; Yang et al., 2009), the AAE values observed here were much lower than those. Although a wide range of AAE values (e.g., from 1.0 to 3.2) have been reported for residential coal combustion (Bond et al., 2002; Sun et al., 2017), the AAE values tend to resemble more those typically associated with biomass burning ($AAE > 1$) than those with fossil fuel/traffic ($AAE \approx 1$) emissions. Presumably, the difference in AAE between coal combustion in residential stoves (poor combustion) and power plants (highly optimized combustion) originates from the effectiveness of combustion, emission

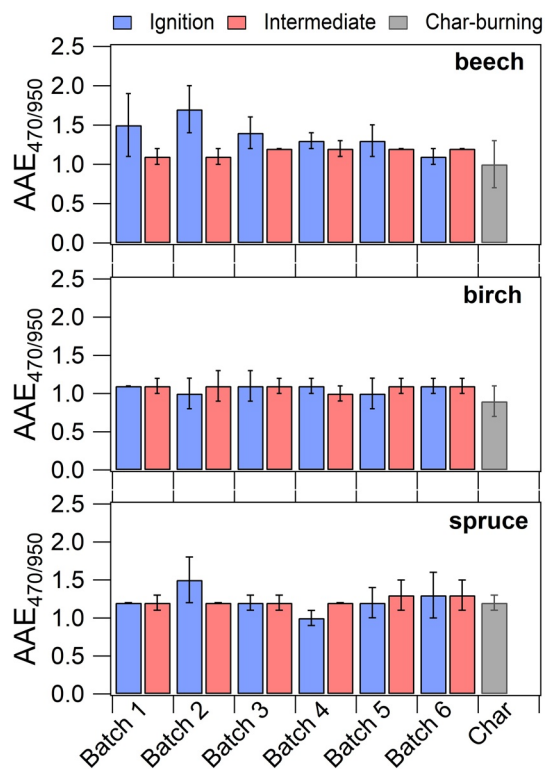


Figure 5. Average $AAE_{470/950}$ values presented for each batch and final char-burning phase according to each logwood combustion experiment (masonry heater). The ignition phase AAE values are calculated by taking into account the first few minutes at the beginning of each batch addition. The intermediate phase demonstrates the combustion period between the batch additions excluding the ignition phase. The char-burning phase demonstrates the final 45 min of the burn-cycle.

(Grieshop et al., 2017; Kumar et al., 2018; Martinsson et al., 2015; Pokhrel et al., 2016; Roden et al., 2006; Saleh et al., 2013; Tasoglou et al., 2017). Of the wood burning studies conducted by using small-scale wood combustion appliances, the study by Martinsson et al. (2015), who used a traditional Scandinavian wood stove and birch logwoods as fuel, bared the closest resemblance to our experimental setup. They also observed relatively low AAE values in fresh emissions (burn cycle average $AAE_{370/950} = 0.9-1.3$), ranging from 1.0 to 1.2 during the flaming phase combustion to 2.5–2.7 during the ignition phase of one batch combustion (Martinsson et al., 2015).

Also in our experiments, the variation of $AAE_{470/950}$ and $b_{abs}(880 \text{ nm})$ was notable within the combustion period (Figures S10–S14), especially during the masonry heater batch combustion conditions. Figure 5 shows the average $AAE_{470/950}$ values during the different phases of the burn cycle from the masonry heater experiments. Of the different logwood species tested, only beech showed some sort of consistency between the different burn phases and batch additions. The $AAE_{470/950}$ values were generally higher during the ignition phase, whereas during the intermediate phases between the batch additions and during the final char-burning phase, the $AAE_{470/950}$ values were slightly lower (Figures 5 and S10). With the other two logwood species tested, no distinct trend could be identified between the different burn phases.

One common feature in all of the masonry heater experiments was the low $b_{abs}(\lambda)$ levels and the highly variable AAE values during the final char-burning phase (Figures S10–S12). The char-burning phase produces almost only ash particles and the BC emissions are the lowest during this burn-out period (Kortelainen et al., 2018), which likely explains the observed noisy/variable AAE levels.

treatment and likely from the properties of the coal being combusted, although it is not particularly meaningful to compare these two sectors due to the evident difference in scale.

3.5. AAE Results From the Wood Combustion Emissions

3.5.1. Masonry Heater and Pellet Boiler Results

Higher emissions of many of the studied aerosol components (e.g., OC, elemental carbon (EC), PAHs, and some inorganics) were observed in the masonry heater combustion experiments when compared to the pellet boiler combustion experiments (Czech et al., 2018; Kanashova et al., 2018). For example, both EC and OC emissions were more than one order of magnitude higher in the masonry heater experiments when compared to the optimized pellet boiler combustion experiments (Czech et al., 2018). The average $b_{abs}(\lambda)$ levels from the different combustion appliances and logwood species tested are presented in Figure S9. As shown in Czech et al. (2018), significant differences were observed, e.g., in the emissions of EC and OC, between the different logwood species tested in the masonry heater combustion experiments. The OC/EC ratios were 0.71 ± 0.14 , 0.13 ± 0.02 , and 0.48 ± 0.13 for beech, birch, and spruce, respectively. In addition, during the masonry heater batch combustion conditions, temporal variation of emissions and the relative chemical composition variation of aerosol species were observed to be significant (Kortelainen et al., 2018).

As can be seen in Figure 2 and Table S4, the variation of AAE values between the different combustion appliances and logwood species tested was quite modest. In the emissions from the masonry heater, the $AAE_{470/950}$ was on average 1.2 ± 0.1 . In the emissions from the pellet boiler, the $AAE_{470/950}$ was higher during normal operation (1.4 ± 0.1) than during unoptimized combustion (1.2 ± 0.0) conditions. These average AAE values representing the whole burn cycle were quite similar to those observed in previous wood combustion studies for fresh emissions

3.5.2. Sauna Stove Results

Two sauna stoves were tested and the emissions from the two stoves were quite different (see Section 2.1.4.2 and Tissari et al. (2019)). Sauna stove 2 produced substantially higher PM, EC and OC concentrations when compared to stove 1 (Tissari et al., 2019). The measured EC and OC concentrations were 3- and 24-fold higher with stove 2 than with stove 1, respectively. Similarly, the measured average $b_{\text{abs}}(\lambda)$ levels were much higher in the emissions of stove 2 than stove 1 (Figures S15). Typically, sauna stoves emit higher concentrations of PM and BC as compared to almost any other residential combustion appliance used (Savolahti et al., 2016; Tissari et al., 2007).

In Figure S16 are shown the burn cycle time series of $b_{\text{abs}}(880 \text{ nm})$ and $\text{AAE}_{470/950}$ from both sauna stoves and from all of the repetitions. Even though the temporal variation of $b_{\text{abs}}(880 \text{ nm})$ and $\text{AAE}_{470/950}$ were notable in the emissions, the $\text{AAE}_{470/950}$ values were similar on average in the emissions from both stoves (Figure 2). Overall, the sauna stove AAE values were similar to the AAE values observed above in the modern masonry heater and pellet boiler emissions.

As can be seen in the burn cycle time series (Figure S16), the $\text{AAE}_{470/950}$ values were highly variable at the end of each batch combustion, during which the $b_{\text{abs}}(880 \text{ nm})$ levels were also the lowest. If taking into account only the $b_{\text{abs}}(880 \text{ nm}) < 40\text{th}$ percentile data, the corresponding burn period average $\text{AAE}_{470/950}$ were 1.3 ± 0.1 and 1.8 ± 0.3 for stove 1 and stove 2, respectively (Table S4). In contrast, for the $b_{\text{abs}}(880 \text{ nm}) \geq 40\text{th}$ percentile data the $\text{AAE}_{470/950}$ values were lower, down to 1.2–1.3 for both stoves (Table S4). This demonstrates that at times when the $b_{\text{abs}}(880 \text{ nm})$ levels are high, the AAE values are relatively low during the burn cycle. Accordingly, when the $b_{\text{abs}}(880 \text{ nm})$ levels are the lowest and noisy, the AAE variation is large, but subsequently the AAE shifts on average toward higher AAE values (particularly in the stove 2 case). The char-burning phases with the lowest levels of $b_{\text{abs}}(880 \text{ nm})$ generate mostly ash particles consisting of alkali metal salts, and the BC emissions are the lowest during this burn-out period (Kortelainen et al., 2018).

3.6. Relevance and Implications of the Observations

To give some perspective to the results presented in this study, Figure 6 shows the average $\text{AAE}_{470/950}$ and $b_{\text{abs}}(880 \text{ nm})$ values from selected primary emission sources covered in this study. The error bars represent the estimated relative uncertainties based on Table 2/Figure S1 applied at $\Delta\text{ATN} = 0.1$ and at the highest time resolution, so here an overestimate was used timewise (for sauna stove the intermediate ATN range uncertainty was used, Figure S1f). The size of the marker in Figure 6 is related to the dilution ratio used in the measurements (the larger the size of the marker, the higher the dilution ratio). In general, there seems to be little relationship between the $b_{\text{abs}}(880 \text{ nm})$ and AAE if excluding the few outlier cases (ethanol bus and power plant with FGD + FF on). As can be seen in Figure 6, most of the average $\text{AAE}_{470/950}$ values were within 1.0 ± 0.4 . If taking into account the δAAE , the differences between the emission sources could be considered negligible. Despite the high uncertainty, previous literature measurements complement these presented average AAE values. For example, as discussed in the previous sections, similar AAE values have been observed in shipping and wood combustion emissions (see Figure 2).

Considering the results shown in Figure 6 in view of the source apportionment of BC/CM, in particular when using the Aethalometer model (see Introduction section), it seems that the selection of AAE values ($\text{AAE}_{\text{FF}}/\text{AAE}_{\text{BB}}$) to be used for the apportionment of carbonaceous matter can be cumbersome based on these results from fresh emissions. Our results demonstrate AAE values in fresh aerosols close to unity even from wood combustion sources (although the burn cycle phase plays a central role in this) and on the contrary AAE values close to two from ship emissions. Similar observations have been reported as well in previous wood combustion and ship emission studies (see e.g., Figure 2) (Corbin et al., 2018; Kumar et al., 2018; Martinsson et al., 2015; Roden et al., 2006; Streibel et al., 2017). These presented examples are relevant, considering that the PM and BC emissions from these sources can be relatively high even on a global scale (Klimont et al., 2017). In principle, in this case for fresh emissions, the source apportionment would fail in accounting for fossil fuel and wood combustion sources. However, obviously, the ambient aerosols are a mixture (internal and external) of primary and secondary aerosols and not solely consisting of freshly emitted aerosols. Therefore, the AAE values in aged emissions can be significantly different than those presented here for the freshly emitted aerosols. However, predicting the effect of aging on AAE values

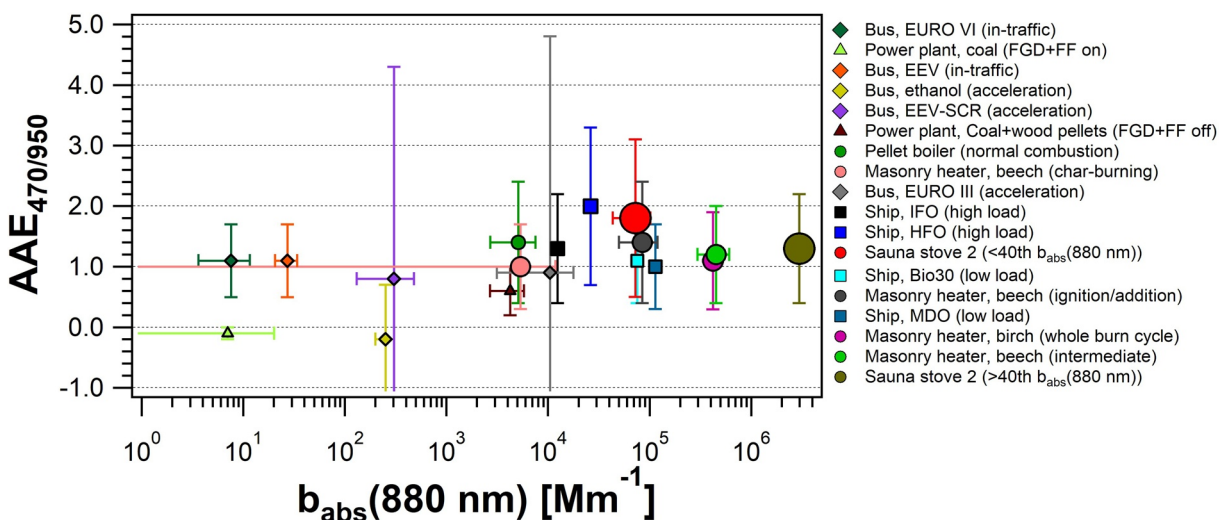


Figure 6. The variation of $AAE_{470/950}$ and $b_{abs}(880 \text{ nm})$ on average in emissions from different sources. The error bars of AAE correspond to the estimated relative uncertainty in Table 2 for $\Delta ATN = 0.1$ and for the highest time resolution there. The size of the marker is related to the applied dilution ratio. The dilution ratios ranged from 0 to 778 (the larger the size of the marker, the greater the dilution ratio). The abbreviations and experiments have been described in Sections 2.1 and 3.5.

is challenging since multiple factors affect it (e.g., the chemical and optical properties of the co-emitted pollutants and other pre-existing aerosols forming the potential coating of light-absorbing aerosols and the effect of aging on morphology) (Gyawali et al., 2009; Lack & Cappa, 2010; Li et al., 2016; Liu et al., 2018; Wu et al., 2018). Further studies are warranted in modeling the effect of aging on the AAE values.

The presented results in this study could be applied to some extent to help the speciation of primary emissions. As reported in Pirjola et al. (2015), newer emission class buses (e.g., EEV and EURO VI) have significantly lower BC emissions as compared to the older emission class buses (EURO III and EURO IV). Our results indicated that the emission class does not affect the AAE dramatically as long as the buses are diesel-fueled (AAE is essentially close to unity, Figure 2). Alternative fuel buses had variable AAE values, but the overall BC emissions were significantly lower when compared to their diesel-fueled counterparts (see Pirjola et al., 2015). Typically, the number of ethanol and GNG buses is very low in the traffic fleet and their contribution to BC emissions from traffic can be considered to be extremely low. Most likely, currently, the effect of alternative fuel vehicles will not be significant on the AAE values in traffic-dominated environments (i.e., AAE values will be close to unity even though there are some alternative fuel buses in traffic).

In terms of residential wood combustion, our results demonstrate that at certain phases of the wood-burning cycle, either in the masonry heater or sauna stoves, when the $b_{abs}(880 \text{ nm})$ levels were the highest, the $AAE_{470/950}$ values tended to be on average closer to unity than that typical for AAE_{BB} . Relatively high $AAE_{470/950}$ values in wood combustion-derived aerosols were mainly observed at times of the burn cycle when the $b_{abs}(880 \text{ nm})$ levels were low. These observations are similar as in the literature, that is, flaming phase combustion produces more soot containing aerosols with lower AAE values than the smoldering phase combustion, which in turn contains relatively more brown carbon or other closer to UV wavelengths absorbing components in the emissions (Kirchstetter et al., 2004; Martinsson et al., 2015; Roden et al., 2006). Consequently, the source apportionment of BC/CM might not work adequately since the modern wood combustion appliances tend to emit aerosols with fairly low AAE values on average (Figure 2). However, once emitted these wood combustion derived aerosols go through atmospheric aging processes, and based on some literature studies (Kumar et al., 2018; Saleh et al., 2013; Tasoglou et al., 2017), aged emissions may have higher AAE values than fresh emissions (e.g., due to the coating of BC particles and secondary organic aerosol formation). Also, the wood combustion in stoves might not be as optimal in reality as in our laboratory experiments (e.g., not dry wood or sweep-cared chimneys) which may produce wood burning-derived aerosols with higher AAE values (Tissari et al., 2019). Furthermore, the variation in wood combustion appliance types is very large (e.g., old masonry heaters, masonry ovens, open fireplaces, wood stoves) and

their impacts of AAE values have not been studied. Nonetheless, considering fresh emissions, the results presented here raise awareness of the possible shortcomings when using the Aethalometer model for source apportionment. The source apportionment method may misinterpret the wood combustion derived BC/CM as fossil fuel origin due to the low AAE values in fresh emissions versus the $AAE_{BB} \approx 2.0 \pm 0.4$ typically used for the apportionment of biomass burning.

In practice, the relevance and utilization of these results are ultimately case-specific. The ambient air sampling location and proximity of point sources play a central role in the applicability of these AAE results for source apportionment and aerosol characterization. As mentioned earlier, the presented results are mainly representative of fresh emissions, thus the results benefit directly mainly users who collect their samples near the sources so that the emissions have not aged considerably. For example, sampling sites that are located in the curbside near city traffic, in the harbor/coastal area near shipping activity, in the islands influenced by shipping lanes and shipping plumes, and in residential-detached house areas affected by emissions from modern wood combustion appliances, etc. In such sites, these AAE results may benefit the source apportionment of carbonaceous matter. However, collectively these AAE results for fresh emissions indicate that the chemical evolution after the emissions and the atmospheric processes likely play a major role in the changes in aerosol absorptive properties.

4. Conclusions

The absorption Ångström exponent (AAE) was observed to vary in freshly emitted aerosols originating from different emission sources. The studied emission sources included shipping, coal-fired power plant, different buses, and wood combustion appliances. The highest AAE values were observed in ship exhaust, alternative fuel buses, and wood burning in sauna stove emissions. The lowest AAE values (along with low BC emissions) were observed in coal-fired power plant emissions with desulfurization plant on and in the emissions from ethanol buses upon acceleration. Overall, the AAE values in diesel bus emitted aerosols were close to unity, although the AAE was observed to depend on the driving conditions (lower AAE values during acceleration than during constant driving). Perhaps surprisingly, the wood-burning derived aerosols had fairly low AAE values on average, but the AAE variation was observed to depend on the combustion appliance, wood species being combusted, and especially on the phase of the burn cycle.

The results presented in this study highlight the precautions needed when performing aerosol characterization and source apportionment based on AAE values. Based on these results from fresh emissions, the source apportionment of light-absorbing carbonaceous matter into fossil fuel and wood burning fractions may be biased when considering, for example, the following findings: i) high AAE values in ship emissions when high sulfur content heavy fuel oil was used as fuel (i.e., high AAE values in fresh fossil fuel emissions) ii) relatively low, yet highly variable, AAE values in wood combustion emissions (i.e., low AAE values in fresh biomass burning emissions) and iii) large variation of AAE values from power-plant and alternative fuel buses emissions. These observations, considered with others, highlight the importance of acknowledging the possible shortcomings in some of the currently used carbonaceous matter source apportionment methods. The effect of variable combustion conditions in different appliances and the effect of chemical evolution after emissions needs to be studied further to better understand the robustness and reliability of ambient source apportionment results. Considering the observed high variability of AAE in fresh emissions versus the relatively minor variability observed in ambient air, this compendium of AAE values could be used in further studies to understand the discrepancy among models and ambient observations.

Data Availability Statement

The data set of processed absorption coefficients is available at <https://zenodo.org/record/4563671>. Data is further available through Aakko-Saksa et al. (2016), Pirjola et al. (2015), Järvinen et al. (2019), Mylläri et al. (2019), Reda et al. (2015) and Tissari et al. (2019).

Acknowledgment

The authors gratefully acknowledge support from following projects: Measurement, Monitoring and Environmental Assessment (MMEA), supported by Tekes and coordinated by the Finnish Energy and Environment Cluster - CLEAN Ltd) research program, NABCEA (Novel Assessment of Black Carbon in the Eurasian Arctic - project (Project nro. 296644, Academy of Finland), SIMO (Wood combustion simulator) -project, (A72189, The Regional Council of Pohjois-Savo), KIUAS -project (Emissions from sauna stoves, for details see <http://www.uef.fi/en/web/fine/kiuas>), EL-TRAN (Transition to a resource efficient and climate neutral electricity system, Strategic Research Council at the Academy of Finland, project grant number 314319), “SEA-EFFECTS BC” (Shipping Emissions in the Arctic, Black Carbon, Business Finland), CITYZER (Services for effective decision making and environmental resilience, Business Finland) project, Business Finland and participating companies via BC Footprint project (49,402–201040) and the HICE - Aerosols and Health -project, a Helmholtz Virtual Institute of Complex Molecular Systems in Environmental Health (<https://www.hice-vi.eu/>).

References

Aakko-Saksa, P., Koponen, P., Aurela, M., Vesala, H., Piimäkorpi, P., Murtonen, T., et al. (2018). Considerations in analyzing elemental carbon from marine engine exhaust using residual, distillate and biofuels. *Journal of Aerosol Science*, *126*, 191–204. <https://doi.org/10.1016/j.jaerosci.2018.09.005>

Aakko-Saksa, P., Murtonen, T., Vesala, H., Koponen, P., Nyssönen, S., Puustinen, H., et al. (2016). *Black carbon measurements using different marine fuels*. Paper presented at 28th CIMAC World Congress.

Amanatidis, S., Ntziachristos, L., Karjalainen, P., Saukko, E., Simonen, P., Kuitinen, N., et al. (2018). Comparative performance of a thermal denuder and a catalytic stripper in sampling laboratory and marine exhaust aerosols. *Aerosol Science and Technology*, *52*(4), 420–432. <https://doi.org/10.1080/02786826.2017.1422236>

Andreae, M. O., & Gelencsér, A. (2006). Black carbon or brown carbon? The nature of light-absorbing carbonaceous aerosols. *Atmospheric Chemistry and Physics*, *6*(10), 3131–3148. <https://doi.org/10.5194/acp-6-3131-2006>

Backman, J., Schmeisser, L., Virkkula, A., Ogren, J. A., Asmi, E., Starkweather, S., et al. (2017). On Aethalometer measurement uncertainties and an instrument correction factor for the Arctic. *Atmospheric Measurement Techniques*, *10*, 5039–5062. <https://doi.org/10.5194/amt-10-5039-2017>

Becerril-Valle, M., Coz, E., Prévôt, A. S. H., Močnik, G., Pandis, S. N., Sánchez de la Campa, A. M., et al. (2017). Characterization of atmospheric black carbon and co-pollutants in urban and rural areas of Spain. *Atmospheric Environment*, *169*, 36–53. <https://doi.org/10.1016/j.atmosenv.2017.09.014>

Blanco-Alegre, C., Calvo, A. I., Alves, C., Fialho, P., Nunes, T., Gomes, J., et al. (2020). Aethalometer measurements in a road tunnel: A step forward in the characterization of black carbon emissions from traffic. *The Science of the Total Environment*, *703*, 135483. <https://doi.org/10.1016/j.scitotenv.2019.135483>

Bond, T. C., & Bergstrom, R. W. (2006). Light absorption by carbonaceous particles: An investigative review. *Aerosol Science and Technology*, *40*(1), 27–67. <https://doi.org/10.1080/02786820500421521>

Bond, T. C., Covert, D. S., Kramlich, J. C., Larson, T. V., & Charlson, R. J. (2002). Primary particle emissions from residential coal burning: Optical properties and size distributions. *Journal of Geophysical Research - D: Atmospheres*, *107*(D21). <https://doi.org/10.1029/2001jd000571>

Bond, T. C., Doherty, S. J., Fahey, D. W., Forster, P. M., Berntsen, T., DeAngelo, B. J., et al. (2013). Bounding the role of black carbon in the climate system: A scientific assessment. *Journal of Geophysical Research - D: Atmospheres*, *118*(11), 5380–5552. <https://doi.org/10.1002/jgrd.50171>

Briggs, N. L., & Long, C. M. (2016). Critical review of black carbon and elemental carbon source apportionment in Europe and the United States. *Atmospheric Environment*, *144*, 409–427. <https://doi.org/10.1016/j.atmosenv.2016.09.002>

Caponi, L., Formenti, P., Massabò, D., Di Biagio, C., Cazaunau, M., Panguì, E., et al. (2017). Spectral- and size-resolved mass absorption efficiency of mineral dust aerosols in the shortwave spectrum: a simulation chamber study. *Atmospheric Chemistry and Physics*, *17*(11), 7175–7191. <https://doi.org/10.5194/acp-17-7175-2017>

Corbin, J. C., Pieber, S. M., Czech, H., Zanatta, M., Jakobi, G., Massabò, D., et al. (2018). Brown and black carbon emitted by a marine engine operated on heavy fuel oil and distillate fuels: Optical properties, size distributions, and emission factors. *Journal of Geophysical Research - D: Atmospheres*, *123*, 6175–6195. <https://doi.org/10.1029/2017JD027818>

Crilley, L. R., Bloss, W. J., Yin, J., Beddows, D. C. S., Harrison, R. M., Allan, J. D., et al. (2015). Sources and contributions of wood smoke during winter in London: assessing local and regional influences. *Atmospheric Chemistry and Physics*, *15*(6), 3149–3171. <https://doi.org/10.5194/acp-15-3149-2015>

Czech, H., Miersch, T., Orasche, J., Abbaszade, G., Sippula, O., Tissari, J., et al. (2018). Chemical composition and speciation of particulate organic matter from modern residential small-scale wood combustion appliances. *The Science of the Total Environment*, *612*, 636–648. <https://doi.org/10.1016/j.scitotenv.2017.08.263>

Di Biagio, C., Formenti, P., Cazaunau, M., Panguì, E., Marchand, N., & Doussin, J.-F. (2017). Aethalometer multiple scattering correction Cref for mineral dust aerosols. *Atmospheric Measurement Techniques*, *10*(8), 2923–2939. <https://doi.org/10.5194/amt-10-2923-2017>

Diapouli, E., Kalogridis, A.-C., Markantonaki, C., Vratolis, S., Fetatzis, P., Colombi, C., & Eleftheriadis, K. (2017). Annual Variability of black carbon concentrations originating from biomass and fossil fuel combustion for the suburban aerosol in Athens, Greece. *Atmosphere*, *8*(12), 234. <https://doi.org/10.3390/atmos8120234>

Drinovec, L., Gregorič, A., Zotter, P., Wolf, R., Bruns, E. A., Prévôt, A. S. H., et al. (2017). The filter-loading effect by ambient aerosols in filter absorption photometers depends on the coating of the sampled particles. *Atmospheric Measurement Techniques*, *10*(3), 1043–1059. <https://doi.org/10.5194/amt-10-1043-2017>

Drinovec, L., Močnik, G., Zotter, P., Prévôt, A. S. H., Ruckstuhl, C., Coz, E., et al. (2015). The “dual-spot” Aethalometer: an improved measurement of aerosol black carbon with real-time loading compensation. *Atmospheric Measurement Techniques*, *8*(5), 1965–1979. <https://doi.org/10.5194/amt-8-1965-2015>

Dumka, U. C., Kaskaoutis, D. G., Tiwari, S., Safai, P. D., Attri, S. D., Soni, V. K., et al. (2018). Assessment of biomass burning and fossil fuel contribution to black carbon concentrations in Delhi during winter. *Atmospheric Environment*, *194*, 93–109. <https://doi.org/10.1016/j.atmosenv.2018.09.033>

Forello, A. C., Bernardoni, V., Calzolari, G., Lucarelli, F., Massabò, D., Nava, S., et al. (2019). Exploiting multi-wavelength aerosol absorption coefficients in a multi-time resolution source apportionment study to retrieve source-dependent absorption parameters. *Atmospheric Chemistry and Physics*, *19*, 11235–11252. <https://doi.org/10.5194/acp-19-11235-2019>

Garg, S., Chandra, B. P., Sinha, V., Sarda-Estevé, R., Gros, V., & Sinha, B. (2015). Limitation of the use of the absorption angstrom exponent for source apportionment of equivalent black carbon: A case study from the north west indo-gangetic plain. *Environmental Science and Technology*, *50*(2), 814–824. <https://doi.org/10.1021/acs.est.5b03868>

Goetz, J. D., Giordano, M. R., Stockwell, C. E., Christian, T. J., Maharjan, R., Adhikari, S., et al. (2018). Speciated online PM1 from South Asian combustion sources - Part 1: Fuel-based emission factors and size distributions. *Atmospheric Chemistry and Physics*, *18*(19), 14653–14679. <https://doi.org/10.5194/acp-18-14653-2018>

Grieshop, A. P., Jain, G., Sethuraman, K., & Marshall, J. D. (2017). Emission factors of health- and climate-relevant pollutants measured in home during a carbon-finance-approved cookstove intervention in rural India. *GeoHealth*, *1*(5), 222–236. <https://doi.org/10.1002/2017gh000066>

Guo, X., Nakayama, T., Yamada, H., Inomata, S., Tonokura, K., & Matsumi, Y. (2014). Measurement of the light absorbing properties of diesel exhaust particles using a three-wavelength photoacoustic spectrometer. *Atmospheric Environment*, *94*, 428–437. <https://doi.org/10.1016/j.atmosenv.2014.05.042>

- Gyawali, M., Arnott, W. P., Lewis, K., & Moosmüller, H. (2009). In situ aerosol optics in Reno, NV, USA during and after the summer 2008 California wildfires and the influence of absorbing and non-absorbing organic coatings on spectral light absorption. *Atmospheric Chemistry and Physics*, 9(20), 8007–8015. <https://doi.org/10.5194/acp-9-8007-2009>
- Harrison, R. M., Beddows, D. C. S., Hu, L., & Yin, J. (2012). Comparison of methods for evaluation of wood smoke and estimation of UK ambient concentrations. *Atmospheric Chemistry and Physics*, 12(17), 8271–8283. <https://doi.org/10.5194/acp-12-8271-2012>
- Harrison, R. M., Beddows, D. C. S., Jones, A. M., Calvo, A., Alves, C., & Pio, C. (2013). An evaluation of some issues regarding the use of aethalometers to measure woodsmoke concentrations. *Atmospheric Environment*, 80, 540–548. <https://doi.org/10.1016/j.atmosenv.2013.08.026>
- Healy, R. M., Sofowote, U., Su, Y., Deboz, J., Noble, M., Jeong, C.-H., et al. (2017). Ambient measurements and source apportionment of fossil fuel and biomass burning black carbon in Ontario. *Atmospheric Environment*, 161, 34–47. <https://doi.org/10.1016/j.atmosenv.2017.04.034>
- Herich, H., Hueglin, C., & Buchmann, B. (2011). A 2.5 year's source apportionment study of black carbon from wood burning and fossil fuel combustion at urban and rural sites in Switzerland. *Atmospheric Measurement Techniques*, 4(7), 1409–1420. <https://doi.org/10.5194/amt-4-1409-2011>
- Järvinen, A., Timonen, H., Karjalainen, P., Bloss, M., Simonen, P., Saarikoski, S., et al. (2019). Particle emissions of Euro VI, EEV and retrofitted EEV city buses in real traffic. *Environmental Pollution*, 250, 708–716. <https://doi.org/10.1016/j.envpol.2019.04.033>
- Jereb, B., Batkovič, T., Herman, L., Šipek, G., Kovše, Š., Gregorič, A., & Močnik, G. (2018). Exposure to black carbon during bicycle commuting-alternative route selection. *Atmosphere*, 9(1), 21. <https://doi.org/10.3390/atmos9010021>
- Kanashova, T., Sippula, O., Oeder, S., Streibel, T., Passig, J., Czech, H., et al. (2018). Emissions from a modern log wood masonry heater and wood pellet boiler: Composition and biological impact on air-liquid interface exposed human lung cancer cells. *Journal of Molecular and Clinical Medicine*, 1, 23–35. <https://doi.org/10.31083/jjmcm.2018.01.004>
- Kang, E., Root, M. J., Toohey, D. W., & Brune, W. H. (2007). Introducing the concept of potential aerosol mass (PAM). *Atmospheric Chemistry and Physics*, 7(22), 5727–5744. <https://doi.org/10.5194/acp-7-5727-2007>
- Kirchstetter, T. W., Novakov, T., & Hobbs, P. V. (2004). Evidence that the spectral dependence of light absorption by aerosols is affected by organic carbon. *Journal of Geophysical Research*, 109(D21), a–n. <https://doi.org/10.1029/2004JD004999>
- Kirchstetter, T. W., & Thatcher, T. L. (2012). Contribution of organic carbon to wood smoke particulate matter absorption of solar radiation. *Atmospheric Chemistry and Physics*, 12(14), 6067–6072. <https://doi.org/10.5194/acp-12-6067-2012>
- Klimont, Z., Kupiainen, K., Heyes, C., Purohit, P., Cofala, J., Rafaj, P., et al. (2017). Global anthropogenic emissions of particulate matter including black carbon. *Atmospheric Chemistry and Physics*, 17(14), 8681–8723. <https://doi.org/10.5194/acp-17-8681-2017>
- Kortelainen, M., Jokiniemi, J., Tiitta, P., Tissari, J., Lamberg, H., Leskinen, J., et al. (2018). Time-resolved chemical composition of small-scale batch combustion emissions from various wood species. *Fuel*, 233, 224–236. <https://doi.org/10.1016/j.fuel.2018.06.056>
- Kumar, N. K., Corbin, J. C., Bruns, E. A., Massabó, D., Slowik, J. G., Drinovec, L., et al. (2018). Production of particulate brown carbon during atmospheric aging of residential wood-burning emissions. *Atmospheric Chemistry and Physics*, 18(24), 17843–17861. <https://doi.org/10.5194/acp-18-17843-2018>
- Lack, D. A., & Cappa, C. D. (2010). Impact of brown and clear carbon on light absorption enhancement, single scatter albedo and absorption wavelength dependence of black carbon. *Atmospheric Chemistry and Physics*, 10(9), 4207–4220. <https://doi.org/10.5194/acp-10-4207-2010>
- Lack, D. A., & Corbett, J. J. (2012). Black carbon from ships: a review of the effects of ship speed, fuel quality and exhaust gas scrubbing. *Atmospheric Chemistry and Physics*, 12(9), 3985–4000. <https://doi.org/10.5194/acp-12-3985-2012>
- Lack, D. A., & Langridge, J. M. (2013). On the attribution of black and brown carbon light absorption using the Ångström exponent. *Atmospheric Chemistry and Physics*, 13(20), 10535–10543. <https://doi.org/10.5194/acp-13-10535-2013>
- Lambe, A. T., Ahern, A. T., Williams, L. R., Slowik, J. G., Wong, J. P. S., Abbatt, J. P. D., et al. (2011). Characterization of aerosol photooxidation flow reactors: heterogeneous oxidation, secondary organic aerosol formation and cloud condensation nuclei activity measurements. *Atmospheric Measurement Techniques*, 4(3), 445–461. <https://doi.org/10.5194/amt-4-445-2011>
- Laskin, A., Laskin, J., & Nizkorodov, S. A. (2015). Chemistry of atmospheric brown carbon. *Chemical Reviews*, 115(10), 4335–4382. <https://doi.org/10.1021/cr5006167>
- Li, J., Liu, C., Yin, Y., & Kumar, K. R. (2016). Numerical investigation on the Ångström exponent of black carbon aerosol. *Journal of Geophysical Research - D: Atmospheres*, 121(7), 3506–3518. <https://doi.org/10.1002/2015jd024718>
- Liu, C., Chung, C. E., Yin, Y., & Schnaiter, M. (2018). The absorption Ångström exponent of black carbon: From numerical aspects. *Atmospheric Chemistry and Physics*, 18(9), 6259–6273. <https://doi.org/10.5194/acp-18-6259-2018>
- Liu, D., Taylor, J. W., Young, D. E., Flynn, M. J., Coe, H., & Allan, J. D. (2015). The effect of complex black carbon microphysics on the determination of the optical properties of brown carbon. *Geophysical Research Letters*, 42(2), 613–619. <https://doi.org/10.1002/2014gl062443>
- Liu, Y., Yan, C., & Zheng, M. (2018). Source apportionment of black carbon during winter in Beijing. *The Science of the Total Environment*, 618, 531–541. <https://doi.org/10.1016/j.scitotenv.2017.11.053>
- Martinsson, J., Abdul Azeem, H., Sporre, M. K., Bergström, R., Ahlberg, E., Öström, E., et al. (2017). Carbonaceous aerosol source apportionment using the Aethalometer model - evaluation by radiocarbon and levoglucosan analysis at a rural background site in southern Sweden. *Atmospheric Chemistry and Physics*, 17(6), 4265–4281. <https://doi.org/10.5194/acp-17-4265-2017>
- Martinsson, J., Eriksson, A. C., Nielsen, I. E., Malmberg, V. B., Ahlberg, E., Andersen, C., et al. (2015). Impacts of combustion conditions and photochemical processing on the light absorption of biomass combustion aerosol. *Environmental Science and Technology*, 49(24), 14663–14671. <https://doi.org/10.1021/acs.est.5b03205>
- Moosmüller, H., Chakrabarty, R. K., & Arnott, W. P. (2009). Aerosol light absorption and its measurement: A review. *Journal of Quantitative Spectroscopy and Radiative Transfer*, 110(11), 844–878. <https://doi.org/10.1016/j.jqsrt.2009.02.035>
- Mueller, L., Jakobi, G., Czech, H., Stengel, B., Orasche, J., Arteaga-Salas, J. M., et al. (2015). Characteristics and temporal evolution of particulate emissions from a ship diesel engine. *Applied Energy*, 155, 204–217. <https://doi.org/10.1016/j.apenergy.2015.05.115>
- Mylläri, F. (2018). From boiler to atmosphere: Effect of fuel choices on particle emissions from real-scale power plants, (Doctoral dissertation). Tampere University of Technology. Retrieved from TUTCRIS research portal. <http://urn.fi/URN:ISBN:978-952-15-4214-5>
- Mylläri, F., Karjalainen, P., Taipale, R., Aalto, P., Häyrynen, A., Rautiainen, J., et al. (2017). Physical and chemical characteristics of flue-gas particles in a large pulverized fuel-fired power plant boiler during co-combustion of coal and wood pellets. *Combustion and Flame*, 176, 554–566. <https://doi.org/10.1016/j.combustflame.2016.10.027>
- Mylläri, F., Pirjola, L., Lihavainen, H., Asmi, E., Saukko, E., Laurila, T., et al. (2019). Characteristics of particle emissions and their atmospheric dilution during co-combustion of coal and wood pellets in a large combined heat and power plant. *Journal of the Air & Waste Management Association*, 69(1), 97–108. <https://doi.org/10.1080/10962247.2018.1521349>

- Olson, M. R., Victoria Garcia, M., Robinson, M. A., Van Rooy, P., Dietenberger, M. A., Bergin, M., & Schauer, J. J. (2015). Investigation of black and brown carbon multiple-wavelength-dependent light absorption from biomass and fossil fuel combustion source emissions. *Journal of Geophysical Research - D: Atmospheres*, *120*(13), 6682–6697. <https://doi.org/10.1002/2014jd022970>
- Pirjola, L., Dittrich, A., Niemi, J. V., Saarikoski, S., Timonen, H., Kuuluvainen, H., et al. (2015). Physical and chemical characterization of real-world particle number and mass emissions from city buses in Finland. *Environmental Science and Technology*, *50*(1), 294–304. <https://doi.org/10.1021/acs.est.5b04105>
- Pokhrel, R. P., Wagner, N. L., Langridge, J. M., Lack, D. A., Jayarathne, T., Stone, E. A., et al. (2016). Parameterization of single-scattering albedo (SSA) and absorption Ångström exponent (AAE) with EC/OC for aerosol emissions from biomass burning. *Atmospheric Chemistry and Physics*, *16*(15), 9549–9561. <https://doi.org/10.5194/acp-16-9549-2016>
- Rajesh, T. A., & Ramachandran, S. (2017). Characteristics and source apportionment of black carbon aerosols over an urban site. *Environmental Science & Pollution Research*, *24*(9), 8411–8424. <https://doi.org/10.1007/s11356-017-8453-3>
- Reda, A. A., Czech, H., Schnelle-Kreis, J., Sippula, O., Orasche, J., Weggler, B., et al. (2015). Analysis of gas-phase carbonyl compounds in emissions from modern wood combustion appliances: influence of wood type and combustion appliance. *Energy & Fuels*, *29*(6), 3897–3907. <https://doi.org/10.1021/ef502877c>
- Resquin, M. D., Santágata, D., Gallardo, L., Gómez, D., Rössler, C., & Dawidowski, L. (2018). Local and remote black carbon sources in the metropolitan area of Buenos Aires. *Atmospheric Environment*, *182*, 105–114
- Robinson, A. L., Donahue, N. M., Shrivastava, M. K., Weitkamp, E. A., Sage, A. M., Grieshop, A. P., et al. (2007). Rethinking organic aerosols: Semivolatile emissions and photochemical aging. *Science*, *315*, 1259–1262. <https://doi.org/10.1126/science.1133061>
- Roden, C. A., Bond, T. C., Conway, S., & Pineda, A. B. O. (2006). Emission factors and real-time optical properties of particles emitted from traditional wood burning cookstoves. *Environmental Science and Technology*, *40*(21), 6750–6757. <https://doi.org/10.1021/es052080i>
- Saarikoski, S., Timonen, H., Carbone, S., Kuuluvainen, H., Niemi, J. V., Kousa, A., et al. (2017). Investigating the chemical species in sub-micron particles emitted by city buses. *Aerosol Science and Technology*, *51*(3), 317–329. <https://doi.org/10.1080/02786826.2016.1261992>
- Saleh, R., Hennigan, C. J., McMeeking, G. R., Chuang, W. K., Robinson, E. S., Coe, H., et al. (2013). Absorptivity of brown carbon in fresh and photo-chemically aged biomass-burning emissions. *Atmospheric Chemistry and Physics*, *13*(15), 7683–7693. <https://doi.org/10.5194/acp-13-7683-2013>
- Sandradewi, J., Prévôt, A. S. H., Szidat, S., Perron, N., Alfarra, M. R., Lanz, V. A., et al. (2008). Using aerosol light absorption measurements for the quantitative determination of wood burning and traffic emission contributions to particulate matter. *Environmental Science and Technology*, *42*(9), 3316–3323. <https://doi.org/10.1021/es702253m>
- Sandradewi, J., Prévôt, A. S. H., Weingartner, E., Schmidhauser, R., Gysel, M., & Baltensperger, U. (2008). A study of wood burning and traffic aerosols in an Alpine valley using a multi-wavelength Aethalometer. *Atmospheric Environment*, *42*(1), 101–112. <https://doi.org/10.1016/j.atmosenv.2007.09.034>
- Savolahti, M., Karvosenoja, N., Tissari, J., Kupiainen, K., Sippula, O., & Jokiniemi, J. (2016). Black carbon and fine particle emissions in Finnish residential wood combustion: Emission projections, reduction measures and the impact of combustion practices. *Atmospheric Environment*, *140*, 495–505. <https://doi.org/10.1016/j.atmosenv.2016.06.023>
- Streibel, T., Schnelle-Kreis, J., Czech, H., Harndorf, H., Jakobi, G., Jokiniemi, J., et al. (2017). Aerosol emissions of a ship diesel engine operated with diesel fuel or heavy fuel oil. *Environmental Science & Pollution Research*, *24*(12), 10976–10991. <https://doi.org/10.1007/s11356-016-6724-z>
- Sun, J., Zhi, G., Hitznerberger, R., Chen, Y., Tian, C., Zhang, Y., et al. (2017). Emission factors and light absorption properties of brown carbon from household coal combustion in China. *Atmospheric Chemistry and Physics*, *17*(7), 4769–4780. <https://doi.org/10.5194/acp-17-4769-2017>
- Tasoglou, A., Saliba, G., Subramanian, R., & Pandis, S. N. (2017). Absorption of chemically aged biomass burning carbonaceous aerosol. *Journal of Aerosol Science*, *113*, 141–152. <https://doi.org/10.1016/j.jaerosci.2017.07.011>
- Tissari, J., Hytönen, K., Lyyränen, J., & Jokiniemi, J. (2007). A novel field measurement method for determining fine particle and gas emissions from residential wood combustion. *Atmospheric Environment*, *41*(37), 8330–8344. <https://doi.org/10.1016/j.atmosenv.2007.06.018>
- Tissari, J., Väätäinen, S., Leskinen, J., Savolahti, M., Lamberg, H., Kortelainen, M., et al. (2019). Fine particle emissions from sauna stoves: Effects of combustion appliance and fuel, and implications for the Finnish emission inventory. *Atmosphere*, *10*(12), 775. <https://doi.org/10.3390/atmos10120775>
- Titos, G., del Águila, A., Cazorla, A., Lyamani, H., Casquero-Vera, J. A., Colombi, C., et al. (2017). Spatial and temporal variability of carbonaceous aerosols: Assessing the impact of biomass burning in the urban environment. *The Science of the Total Environment*, *578*, 613–625. <https://doi.org/10.1016/j.scitotenv.2016.11.007>
- Virkkula, A. (2020). Modeled source apportionment of black carbon particles coated with a light-scattering shell. *Atmospheric Measurement and Techniques: Discussion*, *2020*, 1–25. <https://doi.org/10.5194/amt-2020-438>
- Wu, C., Wu, D., & Yu, J. Z. (2018). Quantifying black carbon light absorption enhancement with a novel statistical approach. *Atmospheric Chemistry and Physics*, *18*(1), 289–309. <https://doi.org/10.5194/acp-18-289-2018>
- Yan, C., Zheng, M., Bosch, C., Andersson, A., Desyaterik, Y., Sullivan, A. P., et al. (2017). Important fossil source contribution to brown carbon in Beijing during winter. *Scientific Reports*, *7*, 43182. <https://doi.org/10.1038/srep43182>
- Yang, M., Howell, S. G., Zhuang, J., & Huebert, B. J. (2009). Attribution of aerosol light absorption to black carbon, brown carbon, and dust in China - interpretations of atmospheric measurements during EAST-AIRE. *Atmospheric Chemistry and Physics*, *9*(6), 2035–2050. <https://doi.org/10.5194/acp-9-2035-2009>
- Zanatta, M., Gysel, M., Bukowiecki, N., Müller, T., Weingartner, E., Areskou, H., et al. (2016). A European aerosol phenomenology-5: Climatology of black carbon optical properties at 9 regional background sites across Europe. *Atmospheric Environment*, *145*, 346–364. <https://doi.org/10.1016/j.atmosenv.2016.09.035>
- Zhu, C.-S., Cao, J.-J., Hu, T.-F., Shen, Z.-X., Tie, X.-X., Huang, H., et al. (2017). Spectral dependence of aerosol light absorption at an urban and a remote site over the Tibetan Plateau. *The Science of the Total Environment*, *590–591*, 14–21. <https://doi.org/10.1016/j.scitotenv.2017.03.057>
- Zotter, P., Herich, H., Gysel, M., El-Haddad, I., Zhang, Y., Močnik, G., et al. (2017). Evaluation of the absorption Ångström exponents for traffic and wood burning in the Aethalometer-based source apportionment using radiocarbon measurements of ambient aerosol. *Atmospheric Chemistry and Physics*, *17*(6), 4229–4249. <https://doi.org/10.5194/acp-17-4229-2017>